RE-EVALUATION OF THE FIRST METAMORPHIC P-T PATH USING QUIG BAROMETRY AND EQUILIBRIUM THERMODYNAMICS

by

Sam Couch

A thesis

submitted in partial fulfillment

of the requirements for the degree of

Master of Science in Geoscience

Boise State University

August 2021

BOISE STATE UNIVERSITY GRADUATE COLLEGE

DEFENSE COMMITTEE AND FINAL READING APPROVALS

of the thesis submitted by

Sam Couch

Thesis Title: Re-evaluation of the First Metamorphic P-T Path Using QuiG Barometry and Equilibrium Thermodynamics

Date of Final Oral Examination: 02 June 2021

The following individuals read and discussed the thesis submitted by student Sam Couch, and they evaluated the student's presentation and response to questions during the final oral examination. They found that the student passed the final oral examination.

Matthew Kohn, Ph.D.	Chair, Supervisory Committee
Adrian Castro, Ph.D.	Member, Supervisory Committee
C.J. Northrup, Ph.D.	Member, Supervisory Committee

The final reading approval of the thesis was granted by Matthew Kohn, Ph.D., Chair of the Supervisory Committee. The thesis was approved by the Graduate College.

DEDICATION

I dedicate this thesis to my family. More specifically, my partner, Britt and my younger brother, Jack for their constant support and motivation. Thank you for pushing me to be the best scientist I can be.

ACKNOWLEDGMENTS

I would like to thank everyone in the Geoscience department at Boise State University, especially my advisor, Dr. Matthew Kohn, who helped me improve my science writing, research abilities, teaching qualifications, and communication skills to become the scientist I am today. I would also like to thank my other committee members, Dr. Adrian Castro, and Dr. C.J. Northrup for their input on both my research and my communication skills. To Dr. Adrian Castro, thank you for all your help with thermodynamic programs and the calculations. My gratitude also goes to Paul Davis for all the help with the Raman microscope and Nick Bulloss for all the help with the Electron Probe. I would also like to thank my graduate peers for all their encouragement throughout the duration of my master's program.

ABSTRACT

Quartz in garnet ("QuiG") barometry is a relatively new technique that uses physical properties of minerals to estimate the pressure of garnet nucleation and growth history independent of chemical equilibrium. QuiG barometry was used to determine pressures of garnet growth and compared to thermodynamically calculated P-T conditions for two samples (FH-1M and Z3H) from the Lower Shieferhülle (Formation), Tauern Window, Austria. FH-1M was the first sample for which a P-T path was calculated through inversion of chemical zoning in garnet (Selverstone et al., 1984). Mineral Assemblage Diagrams (MADs) and geothermobarometric techniques were used to determine P-T conditions for garnet nucleation and peak metamorphism. No MAD reproduced either the results of Selvserstone et al. (1984) or petrologic observations such as mineral assemblages and likely P-T conditions as determined using independent thermobarometers. Thermobarometrically calculated rim conditions were consistent between our study and previous work in the Lower Schieferhülle. However, without appropriate inclusion assemblages and compositions, the accuracy of calculated core P-T conditions could not be independently assessed using thermobarometry for either rock. QuiG isomekes from both samples are broadly consistent with growth of garnet during exhumation with heating as originally proposed by Selverstone et al. (1984). However, the QuiG isomekes for Z3H suggest that 90% or more of the Z3H garnet grew over small changes in pressure and temperature or along a QuiG isomeke (heating with a slight increase in pressure). These results support the accuracy of prior P-T paths and their

tectonic interpretations. However, inconsistencies between QuiG barometry vs. thermodynamic calculations remain unresolved.

TABLE OF CONTENTS

DEDICATION iv

ACKNOWLEDGMENTS v

ABSTRACT vi

TABLE OF CONTENTS viii

LIST OF TABLES x

LIST OF FIGURES xi

LIST OF ABBREVIATIONS xiv

INTRODUCTION 1

BACKGROUND 4

GEOLOGIC BACKGROUND 7

PETROLOGY 11

FH-1M 11

Z3H 16

METHODS 20

Raman Spectroscopy 20

Samples and standards 20

Raman Analyses 22

Peak Fitting 23

Entrapment Pressure Calculations 23

Electron Probe Microanalysis (EPMA): 24
Mineral Assemblage Diagrams (MADs) 26
Thermobarometry 27
Best Case Scenario Expectations 27
RESULTS 29
Zoning Profiles and Thermobarometry 29
QuiG 35
Mineral Assemblage Diagrams 37
DISCUSSION 43
Zoning Profiles & Thermobarometry 43
Consistency of QuiG with the Selverstone et al. (1984) P-T Path 44
MADs 45
What is the correct P-T path? 47
Was there garnet overstepping? 47
CONCLUSIONS AND FUTURE DIRECTIONS 49
REFERENCES 51
APPENDIX 59

LIST OF TABLES

Table A.1. Mineral assemblages in samples FH-1M and Z3H. X's denote presence. Margarite was not directly observed but was reported in Selverstone et al. (1984). 60

Table A.2. Bulk compositions for FH-1M and Z3H using both XMapTools and EDS section scanning technique. * = derived from XMapTools..... 61

Table A.3. Representative garnet compositions normalized to 12 oxygens and mole fractions of X_{Alm}, X_{Prp}, X_{Sps}, and X_{Grs} for FH-1M and Z3H samples. 62

Table A.4. Different thermodynamic programs and their associated solution models used to create mineral assemblage diagrams. 64

Table A.5. Table showing the 128, 206, and 464 peak shifts for each quartz inclusion in the FH-1M garnet. Numbers correspond with inclusion numbers on figure 8. 67

Table A.6. Table showing the 128, 206, and 464 peak shifts for each quartz inclusion in the Z3H garnet. Numbers correspond with inclusion numbers on figure 9..... 68

LIST OF FIGURES

Figure 1. Simplified geologic map of the Tauern Window, Austria (based on Schmid et al., 2013). The sample locations for FH-1M and Z3H are shown by black stars. The sample location for Droop et al. (1985) is located near Gmünd in SE Austria (black box). ZG = Zentralgneis, USH = Upper Schieferhülle, LSH = Lower Schieferhülle, EZ = Eclogite Zone, AA = Austroalpine Unit. 8

Figure 2. Plane-polarized light photomicrograph of FH-1M with points that show maximum entrapment pressure inclusion locations. Blue dot represents the core inclusion, green dot represents the middle inclusion, and the red dot represents the rim inclusion. Labels: Grt = garnet, Hbl = hornblende, Bt = biotite. The matrix consists primarily of plagioclase (Pl), quartz (Qtz), chlorite (Chl), and paragonite (Pg).....12

Figure 3. Plane-polarized light photomicrographs of FH-1M, showing typical textures of kyanite and staurolite and the S1 foliation (black line labeled "S1"). Labels: Hbl = hornblende, Chl = chlorite, Bt = biotite, Pg = paragonite, Pl = plagioclase, Qtz = quartz, Ky = kyanite, St = staurolite. The matrix consists primarily of plagioclase, quartz, chlorite, and paragonite.....13

Figure 4. X-ray maps of garnet from FH-1M showing zoning in Fe, Ca, Mn, and Mg. Small oscillation (black arrow) in Mn profile is ~ 140 μm in width. Black line on Mn profile shows the compositions transect from the EPMA. 15

Figure 5. Photomicrograph of Z3H garnet with points that show maximum entrapment pressure inclusion locations. Blue dot represents the core inclusion, green dot represents the middle inclusion, and the red dot represents the rim inclusion. Labels: Grt = garnet, Pl = plagioclase, Qtz = quartz. The matrix consists primarily of plagioclase and quartz. 17

Figure 6. X-ray maps of garnet from sample Z3H, showing zoning in Fe, Ca, Mn, and Mg. 19

Figure 7. Photomicrographs of FH-1M (left) and Z3H (right) garnets showing the location of all measured quartz inclusions. Numbers correspond with the inclusion number on tables A.5 – A.6. 21

Figure 8. a) Shifts of the 464 cm^{-1} Raman peak of quartz inclusions relative to a standard vs. to their location in the FH-1M host garnet. Blue dots represent inclusions in the 'core', green dots represent inclusions in the 'middle', and red dots are inclusions located in the 'rim'. b) Core-to-rim zoning profile for Ca, Mg, Fe, Fe/(Fe + Mg), and Mn in FH-1M garnet. Traverse distance is ~7 mm. 30

Figure 9. a.) Shifts of the 464 cm^{-1} Raman peak of quartz inclusions relative to a standard vs. their location in the Z3H host garnet. Blue dots represent inclusions in the 'core', green dots represent inclusions in the 'middle', and red dots are inclusions located in the 'rim'. b.) Core-to-rim zoning profile for Ca, Mg, Fe, Fe/(Fe + Mg), and Mn in Z3H garnet. Traverse distance is ~5 mm. 31

Figure 10. Rim thermobarometry for FH-1M showing close overlap among different methods. Colored lines represent specific equilibria calculated by winTWQ. The yellow shaded area from Selverstone et al. (1984) uses older thermobaromtetric calibrations and uses different matrix and rim compositions. 33

Figure 11. Rim thermobarometry for Z3H. The gray lines are the maximum and minimum thermometer lines. Maximum QuiG isomekes for Z3H core (blue), middle (green), and rim (red) quartz inclusions are shown as solid lines. The thickness of each isomeke represents its 300-bar analytical error. 34

Figure 12. Maximum pressure QuiG isomekes for FH-1M (dashed lines) and Z3H (solid lines). Line thickness corresponds with analytical uncertainty (c. 300 bars for FH-1M and Z3H)..... 36

Figure 13. Mineral assemblage diagram for FH-1M whole rock (representative of FH-1M garnet nucleation) with maximum isomekes for FH-1M core (blue), middle (green), and rim (red) quartz inclusions. The thickness of each isomeke represents its 300-bar analytical error. Compositional isopleths for X_{Alm} (0.68) and X_{Grs} (0.16) intersect at ~580˚C and 6.5 kbar (black star), far from any isomeke. 38

Figure 14. Mineral assemblage diagram for FH-1M garnet-free whole-rock (representative of FH-1M garnet rim) with maximum isomekes for FH-1M core (blue), middle (green), and rim (red) quartz inclusions. The thickness of each isomeke represents its 300-bar analytical error=. Compositional isopleths for X_{Alm} (0.65-0.67) and X_{Grs} (0.12) intersect at ~585˚C and 4.5 kbar (black star), several kbar below rim thermobarometric results. Colored boxes represent different thermobarometric methods. None of the assemblages predicted in this MAD corresponds with observations. 39

Figure 15. Mineral assemblage diagram for Z3H whole rock (representative of garnet core conditions) with maximum isomekes for Z3H core (blue), middle (green), and rim (red) quartz inclusions. The thickness of each isomeke represents its 300-bar analytical error. Compositional isopleths for X_{Alm} and X_{Grs} do not intersect. None of the assemblages predicted in this MAD corresponds with observations. 41

Figure 16. Mineral assemblage diagram for Z3H garnet-free whole-rock (representative of garnet rim conditions) with maximum isomekes for Z3H core (blue), middle (green), and rim (red) quartz inclusions. The thickness of each isomeke represents its 300-bar analytical error. Compositional isopleths for X_{Alm} and X_{Grs} do not intersect. None of the assemblages predicted in this MAD corresponds with observations. 42

LIST OF ABBREVIATIONS

EPMA	Electron Probe Microanalyzer/Microanalysis
QuiG	Quartz in Garnet
P-T	Pressure-Temperature
Pinc	Pressure on an inclusion
Ptrap	Entrapment pressure
Ttrap	Entrapment temperature
ZG	Zentralgneis
LSH	Lower Schieferhülle
USH	Upper Schieferhülle

INTRODUCTION

Petrologists seek to quantify the pressure and temperature (P-T) transformations that a rock has experienced. Many different geothermometers and geobarometers have been proposed to help determine peak (maximum) P-T conditions that a rock attained. Determining the P-T transformations of a specific rock or the rock's P-T path can help elucidate the tectonic and thermal evolution of different metamorphic terranes and thus constrain orogenic processes (Spear, Selverstone, Hickmott, Crowley, & Hodges, 1984). The actual P-T path that a rock experienced reflects a relationship between tectonic processes and heat flow (Spear et al., 1984). Chemistry-based thermobarometry using geochemical zoning of minerals like garnet is commonly applied to determine a pressure-temperature (P-T) path of metamorphic rocks (Kohn, 2014b). However, potential biases in traditional, chemistry-based methods can arise if a garnet does not nucleate at the thermodynamically-defined equilibrium reaction ("garnet-in"). Instead, it has been proposed (Pattison, de Capitani, & Gaides, 2011; Spear et al., 2014) that garnet nucleation can occur ≥50 °C above the garnet-in reaction. Hence, more testing is needed to determine if all garnets nucleate outside of thermodynamic equilibrium. Recent studies (e.g., Castro & Spear, 2017; Dragovic, Gatewood, Baxter, & Stowell, 2018) have shown that elastic barometry implies different P-T conditions in the core regions of garnets than inferred using chemically-based methods. However, rim analyses can yield very similar results to thermodynamic methods. Overall, comparing the traditional chemical method

to the new physics-based method will help us identify potential problems in both methods.

With the advent of highly precise Raman microspectroscopy, elastic barometry of mineral inclusions may provide an alternative to chemically based calculations (Enami, Nishiyama, & Mouri, 2007). Rather than relying on chemical equilibrium, this approach utilizes the physical properties of mineral inclusions, more specifically, the P-T dependence of mineral volumes (Angel, Mazzucchelli, Alvaro, Nimis, & Nestola, 2014; Enami et al., 2007; Rosenfeld & Chase, 1961; Zhang, 1998). When an inclusion mineral (e.g., quartz) becomes trapped within a rigid host mineral (e.g., garnet), both experience an identical pressure and temperature, and the cavity in the host exactly matches the size of the inclusion without strain. When the rock begins to exhume, an inclusion with different elastic properties than the host will develop a different pressure compared to the host mineral and accumulate strain (Rosenfeld & Chase, 1961). Raman microspectroscopy quantifies differential strains through shifts in characteristic peak positions of the inclusion (e.g., 464 cm^{-1} for quartz) relative to a standard. Using this differential strain and equations of state for host minerals and inclusion minerals, entrapment pressures of the inclusion can be inferred (Angel et al., 2014; Kohn, 2014a). An understanding of the entrapment pressure from multiple inclusions distributed throughout the garnet (i.e., core to rim) can help determine the P-T path of a specific rock (Ashley, Steele-MacInnis, & Caddick, 2014).

I compared calculated P-T histories using two different methods (physics-based vs. chemistry/thermodynamics based) in this study. I reevaluated the P-T path of rocks from the Tauern Window, Austria, which were investigated by Selverstone, Spear, Franz,

and Morteani (1984), using updated thermodynamic models and Raman spectroscopy. I sought to determine if elastic barometry vs. thermodynamic models would produce different P-T paths outside of analytical and modeling errors of c. 5˚C and 100-200 bars. I also evaluated whether garnets could have grown isothermally and isobarically, as predicted theoretically from reaction overstepping.

BACKGROUND

Thermodynamic inversion of geochemical zoning is one way to quantify a rock's P-T path. Garnet composition depends on the composition of a rock, pressure, and temperature. As pressure and temperature change, garnet composition likewise changes. If a garnet is growing during changes in P and T, changing compositions should be encoded as chemical zoning. If growth occurs at equilibrium, and chemical diffusion is not too fast (temperatures are not too high), the growth zoning can be inverted to infer the P-T path (Spear & Selverstone, 1983). Inversion of chemical zoning, however, assumes that garnet growth always occurs at equilibrium, or that disequilibrium is too small to significantly affect calculations.

Theoretically, crystals cannot nucleate at chemical equilibrium. Nucleation overstepping occurs when a rock crosses into a mineral stability field (crosses its equilibrium isograd reaction), but the mineral does not nucleate. Instead the rock must achieve a P-T condition sufficiently removed from the isograd reaction to overcome a surface free energy barrier. If overstepping occurs, at least some of the zoning recorded within the crystal does not reflect equilibrium growth and therefore cannot reflect equilibrium. Because equilibrium must be assumed to invert chemical zoning, nucleation overstepping implies that at least some portion of a chemically based P-T path must be unreliable (Spear, 2017).

Nucleation overstepping can be described conceptually using crystal nucleation theory. Crystals must grow from initial atomic clusters (called embryos). Any assemblage

of atoms has two Gibbs free energy components: volumetric free energy and surface free energy such that $\Delta G_{total} = \Delta G_{volume} + \Delta G_{surface}$. Surface free energy is always positive and acts to dissolve clusters, and while it does not contribute much to the overall energy of large crystals (>~100 nm diameter), it can strongly influence the free energy of embryos. At an equilibrium reaction (e.g., at a theoretical mineral-in isograd), $\Delta G_{volume} = 0$. Thus, ΔG_{total} is positive, and a crystal cannot form. But as temperature rises, ΔG_{volume} becomes more negative. As ΔG_{volume} becomes more negative, ΔG_{total} develops a maximum at a special radius, called the critical radius (r^*). r^* decreases as the amount of overstepping increases. Thus, for a small amount of overstepping, random clustering of atoms will not reach r^*, and the nucleation of a new crystal will not occur. However, if a larger amount of overstepping takes place, r^* decreases, and random clustering of atoms can cross the Gibbs free energy maximum. At that point, the crystal will grow spontaneously. Because the Gibbs free energy is greater than equilibrium conditions, the crystal will grow at isothermal/isobaric conditions until the excess energy is used. After the excess energy is exhausted all minerals attain chemical equilibrium (at their rims).

Numerous studies use methods that rely on chemical equilibrium without considering the bias of overstepping. Consequently, an independent method that does not rely on chemical equilibrium could provide an unbiased measure of a P-T path. Raman spectroscopy can be used to determine crystal strains. Using equations of state for the inclusion, these strains are inverted to determine an average pressure on the inclusion ("Pinc"). From the equations of state for both the inclusion and host, entrapment pressure (Ptrap) or temperature (Ttrap) of a mineral inclusion can be calculated for an assumed

temperature or pressure. Such estimates then provide an independent alternative to chemically-based estimates.

For this study, I focused on quartz inclusions inside garnet hosts. Quartz and garnet provide a nearly ideal system for estimating Ptrap. Quartz is much more compressible than garnet, so, as the host rock is exhumed, the quartz inclusion expands differentially relative to the garnet host (Rosenfeld & Chase, 1961). This differential pressure induces a compressive strain (residual strain) on the crystal. Residual strain is quantified using the shift in Raman peak positions (128, 206, 464 cm^{-1} peaks; Enami et al., 2007; Kohn, 2014a) as implemented using the StRAinMAN software (Angel, Murri, Mihailova, & Alvaro, 2019). This strain tensor is then converted to an average pressure (Pinc) using an Excel sheet provided by Mateo Alvaro (personal communication, 2018). This newly calculated average pressure is then converted into the entrapment pressure (Ptrap) using garnet and quartz equations of state, as implemented with the EosFitPinc software (Angel, Mazzucchelli, Alvaro, & Nestola, 2017). These pressures and reference temperatures determined through garnets (core, middle, & rim) are compared to P-T paths determined through thermodynamic inversion of garnet chemical zoning.

GEOLOGIC BACKGROUND

The samples I analyzed were collected from the Tauern Window, Austria (Figure 1), by Selverstone et al. (1984). The Tauern Window exposes a Cenozoic nappe with crustal slices that originated from a distal European continental margin and the Valais Ocean (Schmid, Scharf, Handy, & Rosenberg, 2013). This window shows a polyphase metamorphic history with older, high-P, low-T assemblages overprinted by younger lower-P, higher-T assemblages (Droop, 1985; Groß, Pleuger, Handy, Germer, & John, 2020; Selverstone & Spear, 1985; Selverstone et al., 1984). This change in P-T conditions reflects a tectonic shift from subduction to collision (Groß et al., 2020; Selverstone & Spear, 1985; Selverstone et al., 1984; Selverstone, 1985).

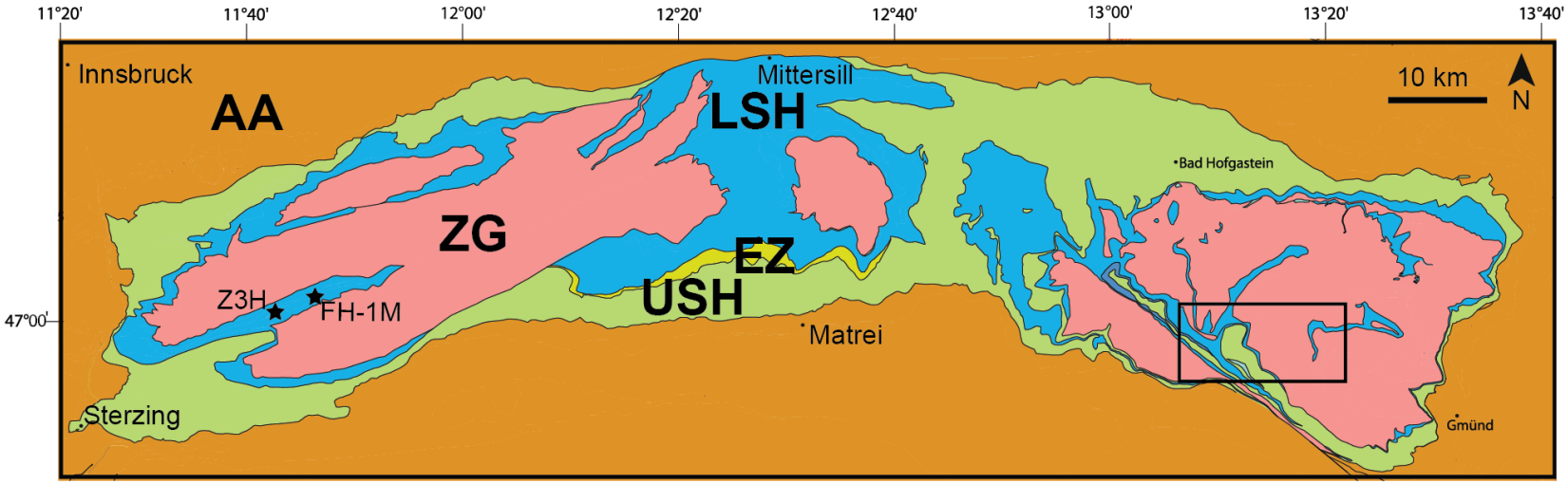

Figure 1. Simplified geologic map of the Tauern Window, Austria (based on Schmid et al., 2013). The sample locations for FH-1M and Z3H are shown by black stars. The sample location for Droop et al. (1985) is located near Gmünd in SE Austria (black box). ZG = Zentralgneis, USH = Upper Schieferhülle, LSH = Lower Schieferhülle, EZ = Eclogite Zone, AA = Austroalpine Unit.

Schmid et al. (2013) proposed a 5-stage tectonic evolution for the Tauern Window: 1) Subduction of the Piemont-Liguria Ocean and the accretion of Austroalpine nappe stack oceanic relics. Sparse ages preclude a robust estimate of the timing of this event. 2) Subduction of the Valais Ocean and the most distal sections of the European margin around 45 Ma and the Subduction of Eclogite Zone rocks beneath the Austroalpine nappe stack around 41 Ma. 3) Exhumation of high-pressure rocks, simultaneous with accretion of the European crust around 35 Ma. 4) Formation of the Venediger Duplex and regional overprinting metamorphism ("Tauernkristallization; Sander, 1911"). 5) The indentation, doming, and overall lateral extension. The Southern Alpine crust east of the Giudicarie Belt began to 'indent' the Eastern Alps by approximately 65km in the N-S direction approximately 23-21 Ma (Linzer, Decker, Peresson, Dell'Mour, & Frisch, 2002). This indentation, along with the subducted supporting lithosphere, caused doming in the Tauern Window as well as the lateral extrusion in this part of the Eastern Alps (Horváth et al., 2006; Lippitsch, Kissling, & Ansorge, 2003; Ratschbacher, Frisch, Linzer, & Merle, 1991; Rosenberg, Brun, Cagnard, & Gapais, 2007; Scharf, Handy, Favaro, Schmid, & Bertrand, 2013).

The rocks exposed in the Tauern Window are divided into three sections: The Zentralgneis (ZG), the Lower Schieferhülle (LSH), and the Upper Schieferhülle (USH). This study examined rocks from the Lower Shieferhülle unit (LSH). The Zentralgneis (ZG) unit is the structurally lowest unit in the area (Cliff, 1981). The primary composition of the unit includes granitic/tonalitic gneisses, migmatites, and pre-Mesozoic intrusives (Cliff, 1981). The ZG unit makes a tectonic contact with the LSH (Ackermand & Raase, 1978; Morteani, 1974). However, the LSH unit is considered an allochthonous

sequence that is distinctive from the ZG intrusive rocks (Selverstone et al., 1984) and contains a wide range of metavolcanic and metasedimentary lithologies that range in age from Paleozoic to Mesozoic (Ackermand & Raase, 1978; Morteani, 1974). The USH unit is the uppermost unit and consists mostly of an allochthonous series of marine metasedimentary and volcanic rocks (Morteani, 1974; Raith, Hormann, & Abraham, 1977). A thin section of eclogites and blueschists occurs between the boundary of the LSH and USH units in the southern Tauern Window, outside the study area.

Selverstone et al. (1984) collected the two samples analyzed in this study – Z3H and FH-1M – in a syncline of LSH flanked by the ZG unit (Figure 1) and provided them to us for study. The P-T conditions for FH-1M, calculated by thermodynamic modeling of chemical zoning in garnet, show a clockwise P-T path (exhumation with heating) with a slight increase in pressure at the start of the P-T path (Selverstone et al., 1984). The high pressures calculated for FH-1M (10 kb at 530˚C) represent the burial of LSH rocks to ~ 35km with a prograde path of heating due to the decay of subduction isotherms (Selverstone et al., 1984).

PETROLOGY

FH-1M

FH-1M is a garbenschist from the LSH (Figure 2). A garbenschist is a rock that contains sheaves ('garben' or bundles) of amphibole that can measure up to 20 cm and develop in the foliation (Selverstone et al., 1984). This sample was selected for study because it was the first rock from which a P-T path was determined using thermodynamic inversion of chemical zoning in garnet (Selverstone et al., 1984). All minerals in this rock (Table A.1) appear to be in textural equilibrium, aside from staurolite, which appears embayed and relict (Figure 3), and fine grained (late stage) chlorite. Kyanite accounts for ~ 1.5% of the matrix, but appears prismatic with no prominent reaction features, suggesting it was in equilibrium with other matrix minerals (Figure 3). This sample preserves evidence for two deformations. An early, strong foliation (S1 = D1) is defined by shape preferred orientation of plagioclase, chlorite, biotite, ilmenite, and fine grained paragonite along plagioclase grain boundaries (Figure 3). S1 anastomoses around plagioclase crystals, but it is not clear if this represents a separate deformational event, and we consider it a single fabric. All porphyroblasts overgrow this foliation statically. Hornblende porphyroblasts show brittle extension (D2). There is a strong foliation preserved through epidote, ilmenite, rutile, and biotite (Selverstone et al., 1984). However, biotite is present both within the matrix (first generation) as well as ‘flakes’ within the hornblende crystals (second generation). Strongly zoned plagioclase crystals up to 3 mm in length populate the FH-1M matrix.

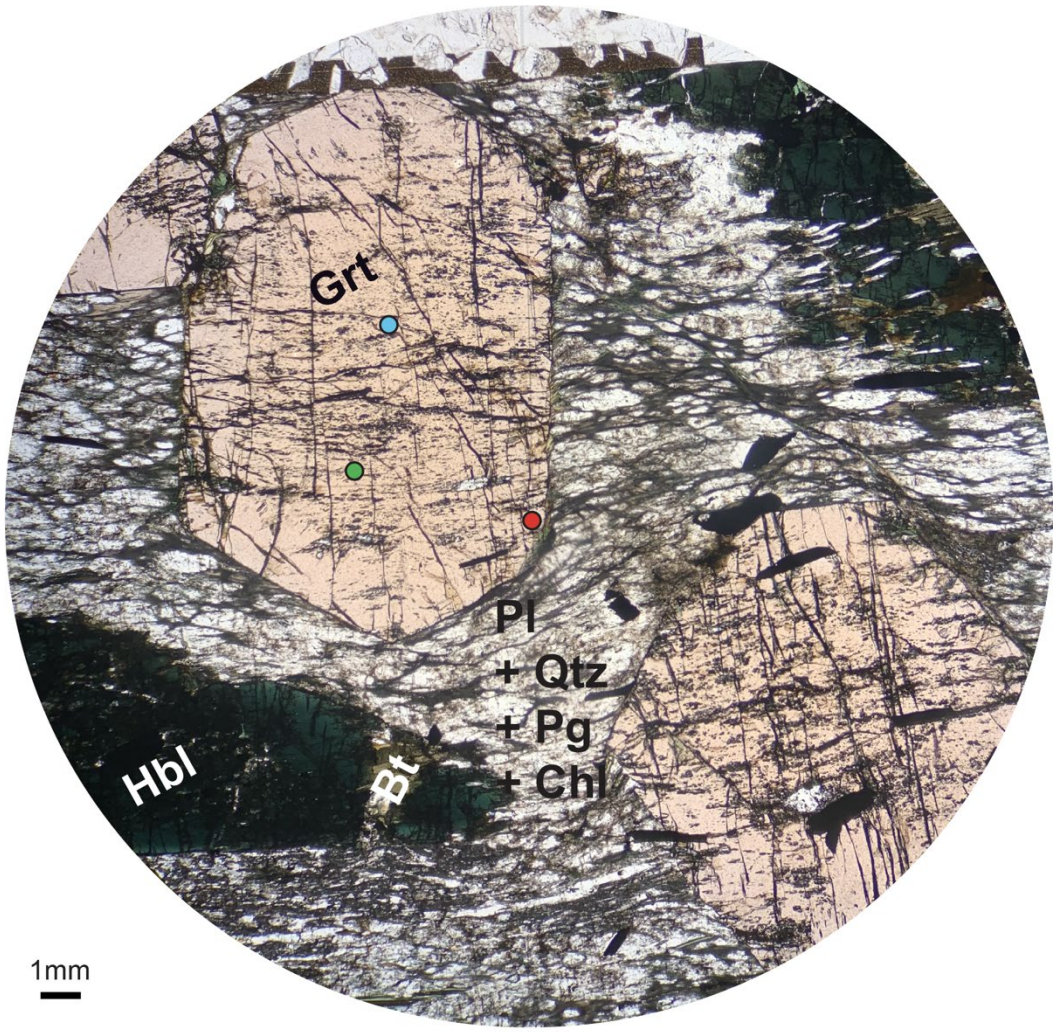

Figure 2. Plane-polarized light photomicrograph of FH-1M with points that show maximum entrapment pressure inclusion locations. Blue dot represents the core inclusion, green dot represents the middle inclusion, and the red dot represents the rim inclusion. Labels: Grt = garnet, Hbl = hornblende, Bt = biotite. The matrix consists primarily of plagioclase (Pl), quartz (Qtz), chlorite (Chl), and paragonite (Pg).

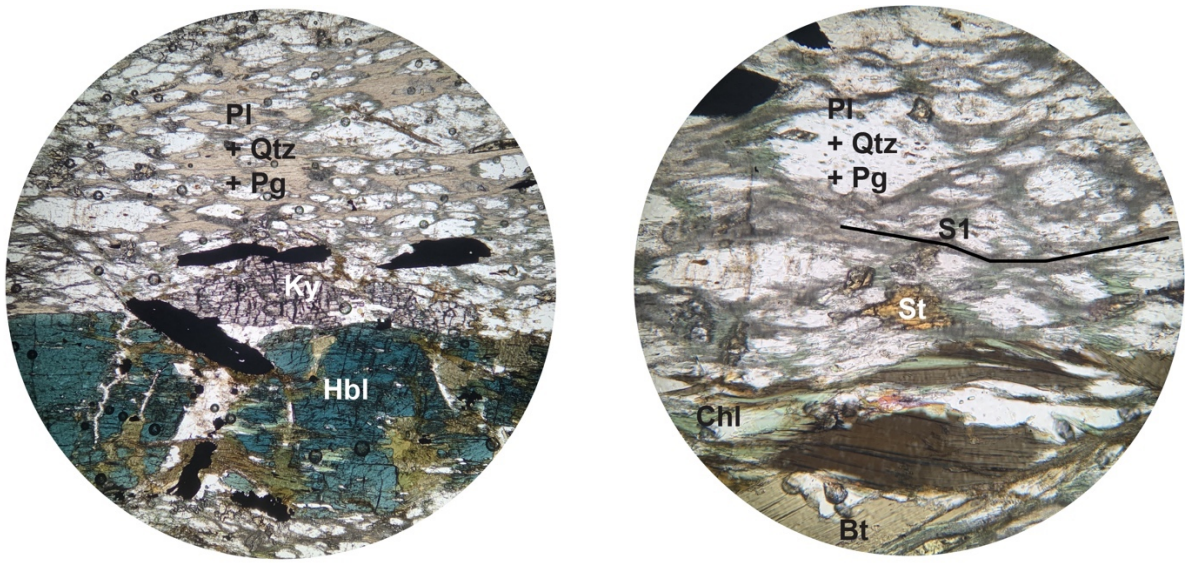

Figure 3. Plane-polarized light photomicrographs of FH-1M, showing typical textures of kyanite and staurolite and the S1 foliation (black line labeled "S1"). Labels: Hbl = hornblende, Chl = chlorite, Bt = biotite, Pg = paragonite, Pl = plagioclase, Qtz = quartz, Ky = kyanite, St = staurolite. The matrix consists primarily of plagioclase, quartz, chlorite, and paragonite.

Large (cm-scale) idioblastic garnets as well as large (cm-scale) amphibole crystals overprint this foliation. In this sample, garnets are highly fractured and contain inclusions of quartz, ankerite, plagioclase, epidote, and ilmenite. Our garnets do not show any rotational fabrics, although other samples from the LSH show syn-deformational rotational fabrics. Garnet zoning profiles in this study and in Selverstone et al. (1984) are similar (Figure 4). The zoning profiles for FH-1M are consistent with preservation of original growth zoning, with a decrease in Mn and increase in Mg towards the rim of the garnet. (Figure 4). Selverstone et al. (1984) calculated rim P-T conditions of 550 ± 25˚C and 7.0 ± 1.0 kbar and a P-T path that shows exhumation with heating. Fine-scale oscillations (ranging from 0.01-0.03 in XSps for a ~140 μm band near the rim of the garnet) in the profiles are consistent with relatively little diffusive smoothing. Bulk compositions and representative garnet analyses for FH-1M are presented in table A.2 and A.3 respectively.

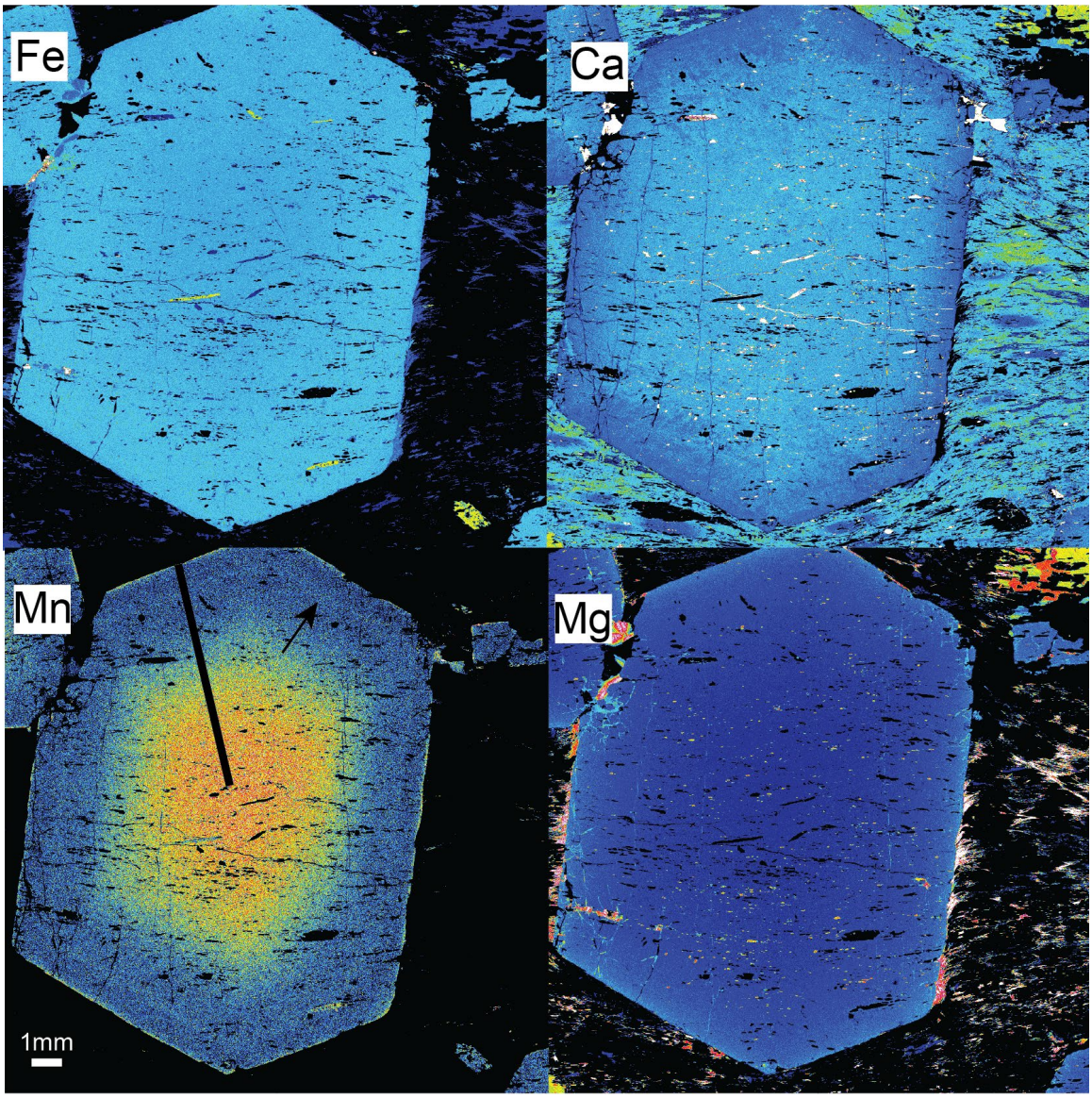

Figure 4. X-ray maps of garnet from FH-1M showing zoning in Fe, Ca, Mn, and Mg. Small oscillation (black arrow) in Mn profile is ~ 140 µm in width. Black line on Mn profile shows the compositions transect from the EPMA.

Z3H

Z3H is a metavolcanic rock with coarse-grained amphibole from the LSH unit (Figure 5). Z3H contains hornblende, garnet, biotite, chlorite, plagioclase, epidote, ankerite, quartz, ilmenite, and cummingtonite. Garnet is porphyroblastic and post-deformational. Hornblende porphyroblasts overprint the matrix fabric and are randomly oriented. A small amount of late-stage cummingtonite (~1 % modal abundance) overgrows the edges of hornblende grains. Z3H garnet contains abundant inclusions of quartz, epidote, ankerite, plagioclase, and ilmenite throughout most of its volume, but does not contain any inclusions in the outermost rim. Matrix minerals consist primarily of plagioclase, biotite and quartz with large crystals of chlorite and hornblende (Figure 5). Unlike FH-1M, Z3H contains no obvious foliation, and plagioclase is uniformly <100 μm in diameter. These differences may suggest different deformational histories, even though both rocks have broadly similar bulk compositions (Table A.2).

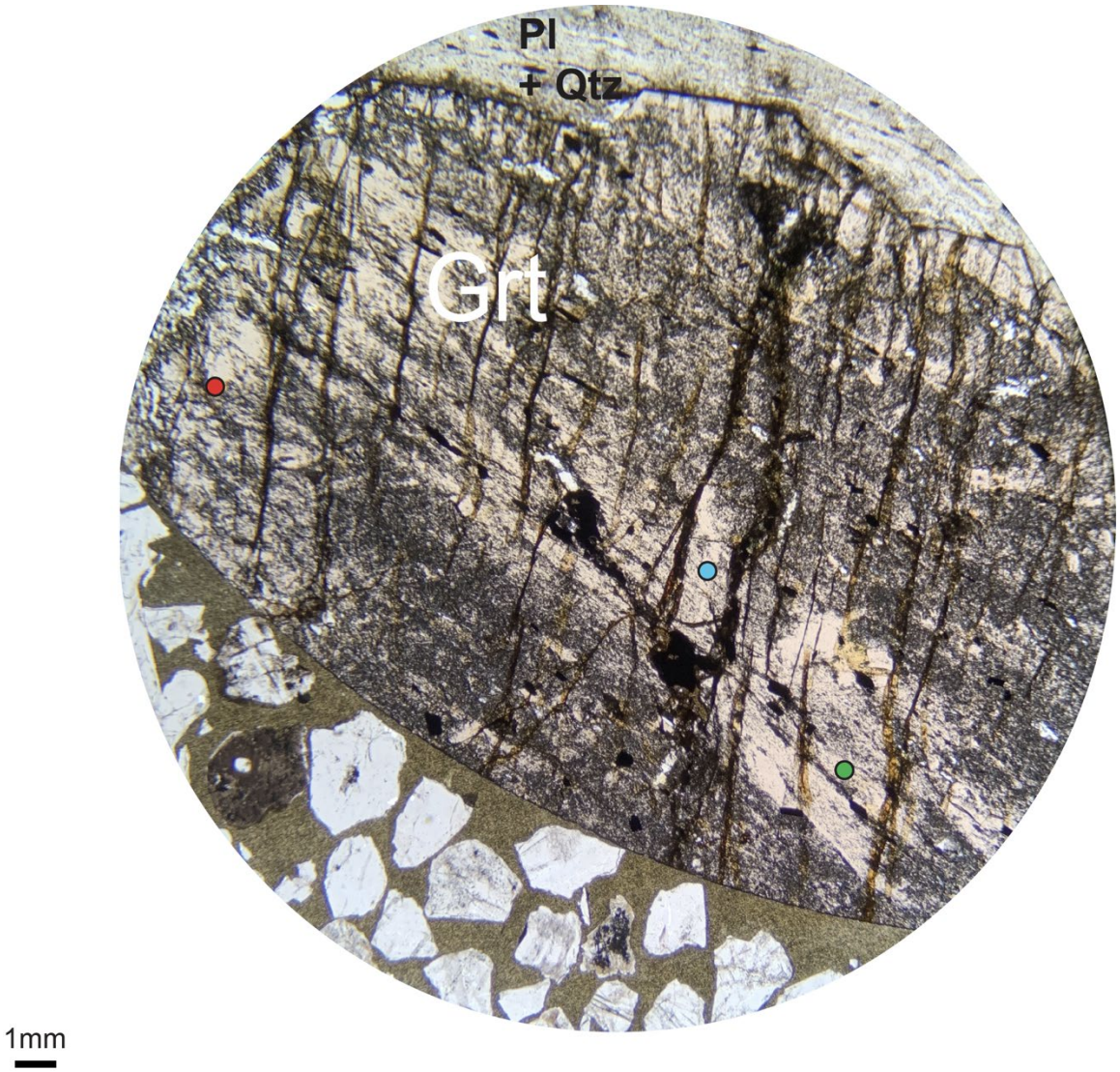

Figure 5. Photomicrograph of Z3H garnet with points that show maximum entrapment pressure inclusion locations. Blue dot represents the core inclusion, green dot represents the middle inclusion, and the red dot represents the rim inclusion. Labels: Grt = garnet, Pl = plagioclase, Qtz = quartz. The matrix consists primarily of plagioclase and quartz.

Garnet zoning profiles for Z3H are shallow throughout, except for the outermost (100μm) inclusion-free rim where the profiles steeply increase for Mg and Fe (increasing) and steeply decrease for Ca and Fe/(Fe + Mg) (Figure 6). Original growth zoning appears to be preserved with a decrease in Mn towards the rim and an increase in Mg towards the rim. Selverstone et al. (1984) did not calculate rim P-T conditions or a P-T path for Z3H. Bulk compositions and representative garnet analyses for Z3H are presented in table A.2 and A.3 respectively.

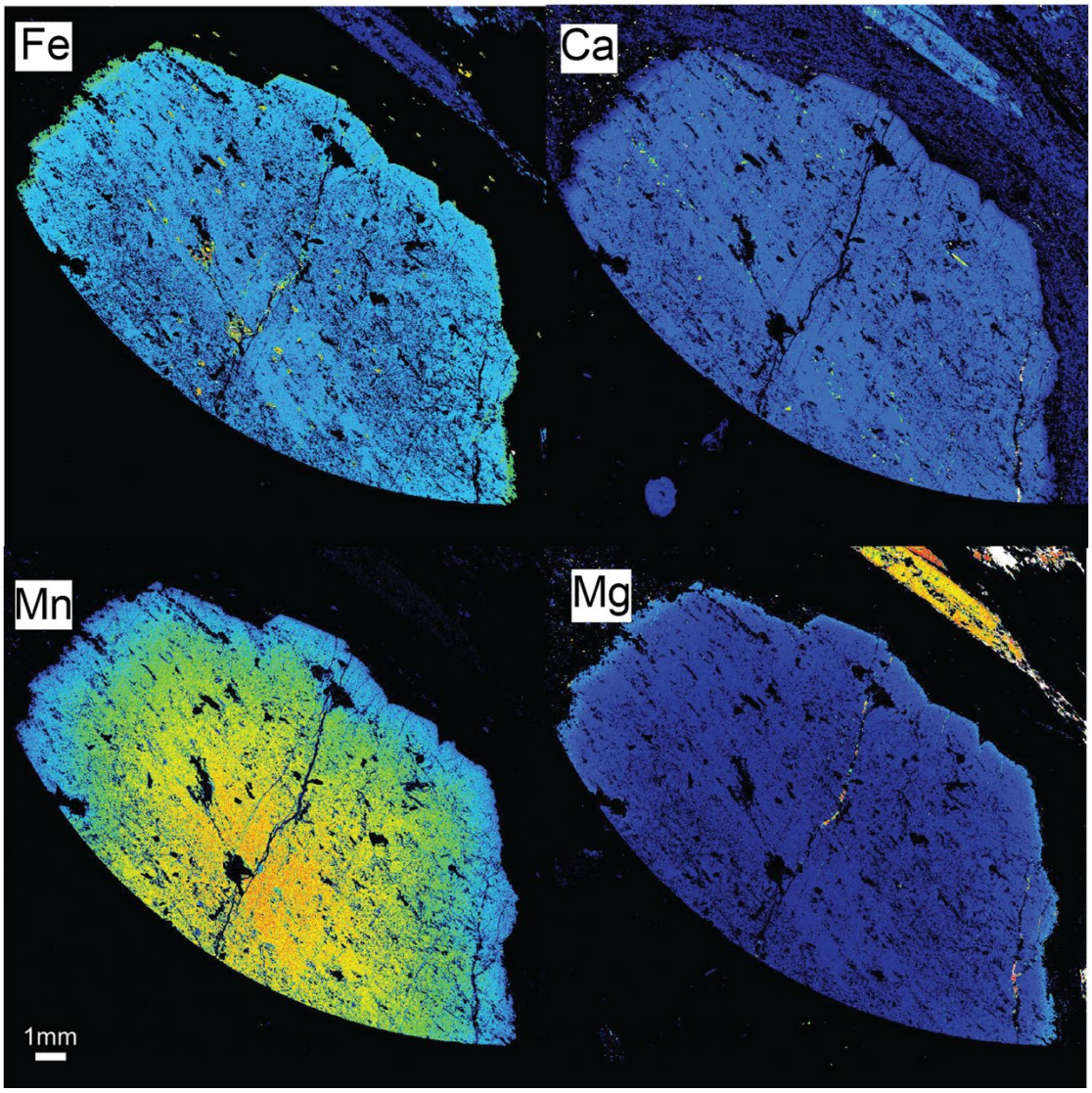

Figure 6. X-ray maps of garnet from sample Z3H, showing zoning in Fe, Ca, Mn, and Mg.

METHODS

Raman Spectroscopy

Samples and standards

Polished, 100-µm thick sections for both samples were obtained commercially to enable collection of Raman spectra on inclusions and EPMA data from the same areas. Our reference standards for Raman spectra were stress-free crystals of Herkimer quartz. These quartz standards were cut into slices, polished, and mounted in putty to reduce stress gradients across the crystals. A total of 10 quartz inclusions were located and analyzed for FH-1M and a total of 31 quartz inclusions were located and analyzed for Z3H (Figure 7).

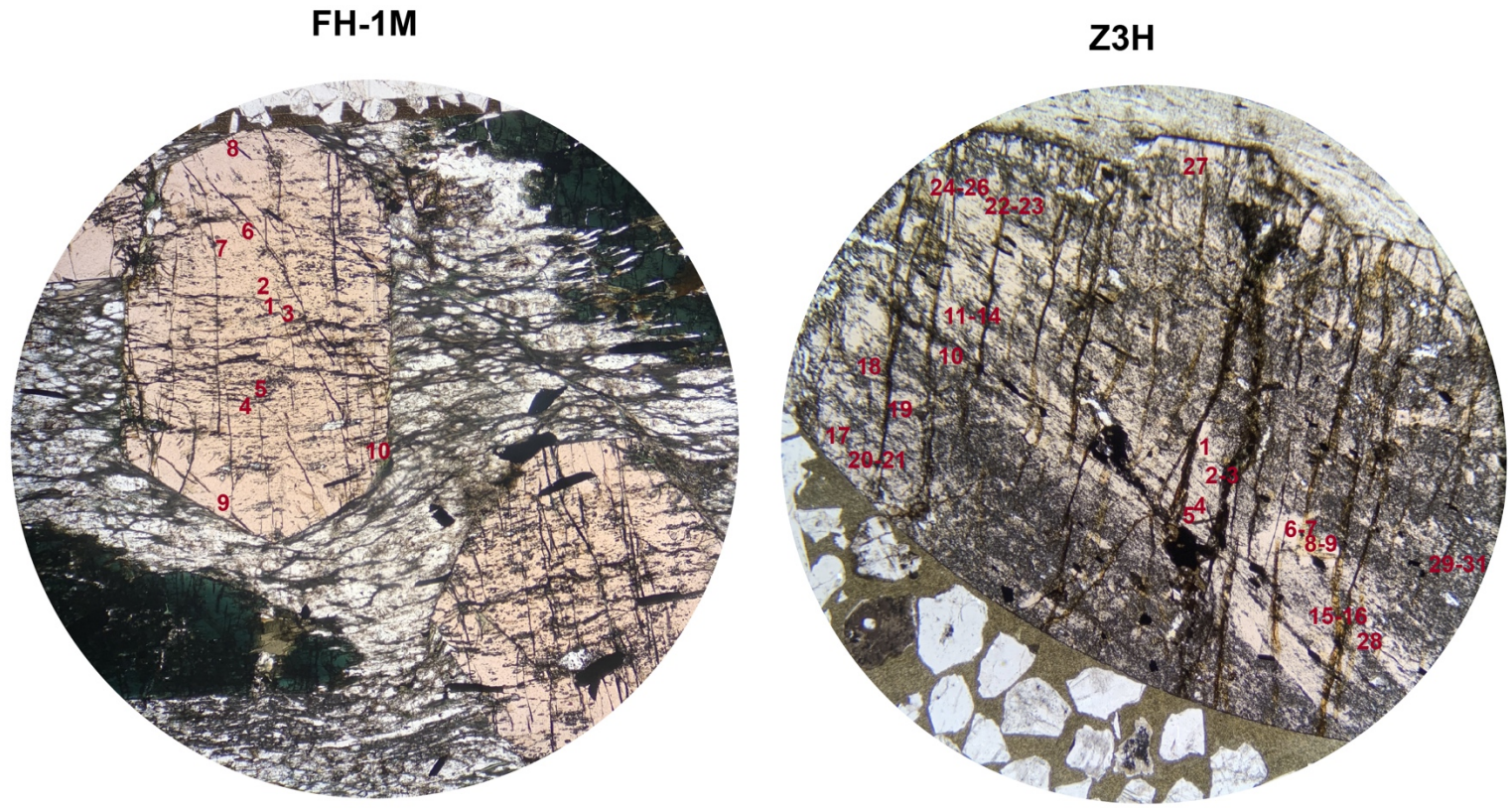

Figure 7. Photomicrographs of FH-1M (left) and Z3H (right) garnets showing the location of all measured quartz inclusions. Numbers correspond with the inclusion number on tables A.5 – A.6.

Raman Analyses

Raman spectra of quartz inclusions were collected using a Horiba LabRam confocal microRaman system with a frequency-doubled Nd:YAG (Green, 532 nm) laser, housed in the Materials Science and Engineering Department, Boise State University. Before using the Raman microscope, the laser was warmed up for a minimum of one hour to ensure laser stability (Cizina, 2020). An initial instrument calibration was performed using a Si wafer. We shined a mercury vapor lamp on both samples to introduce a fixed (~484 cm^{-1}) vibrational band that could be used to monitor instrumental drift independent of our quartz standard. Specific analytical parameters included: a thermoelectrically cooled charge-coupled device (CCD) with an 800 mm focal length, a diffraction grating resolution of 1,800 line/mm, a fixed 100 µm aperture size (provides a spatial resolution of ~0.5 cm^{-1} for the green laser), a spectral range of 100-1100 cm^{-1} (to ensure analysis of the three quartz peaks and the mercury line (128 cm^{-1}, 206 cm^{-1}, and 464 cm^{-1}; 484 cm^{-1}), a single spectral acquisition time of 10 seconds, and 3 accumulations of spectra (30s total data collection). The mercury light source was an artificial source from an external light placed adjacent to the Raman microscope. Data were collected without overhead fluorescent lights to reduce external light interference. Once the machine was calibrated, a quartz standard reference was analyzed for its Raman spectra. Boise State's Raman microscope has a peak reproducibility of ±0.1 cm^{-1} (128 and 464 peaks) and ±0.2 cm^{-1} (206 peak) (Cizina, 2020).

Inclusions for FH-1M were first located using the Raman microscope and a petrographic microscope for Z3H. I selected inclusions with low aspect ratio that were fully entrapped in the garnet and distant from any other inclusions, cracks, or surfaces;

these conditions ensure the most accurate calculated entrapment conditions (Campomenosi et al., 2018; Mazzucchelli et al., 2018; Murri et al., 2018). Inclusions were located throughout the entire garnet (core, middle, rim) to determine the pressure change throughout the garnet's growth. Inclusions were analyzed at 100X magnification, and a reference quartz standard spectrum was collected immediately after each measurement to ensure that the laser did not drift during data acquisition.

Peak Fitting

The principal quartz peaks in the Raman spectrum at approximately 128, 206, and 464 cm^{-1} were fitted using an in-house MATLAB® code that used a non-linear least-squares curve-fitting method (Cizina, 2020). These peaks were fit using Lorentzian, Gaussian, or a combination of the two functions, depending on the quality of fit for each peak. To optimize the fitting, the code performs an automated baseline correction of the Raman spectra (Al-Rumaithi, 2020), isolates the specific spectral range needed for the analyses to define initial fitting parameters (intensity, location, width), and uses the MATLAB® Curve Fitting toolbox with the initial fitting parameters to generate the three different functions which are later returned as the best fit for the estimated peak positions and their associated root mean square error (Cizina, 2020). These peak fits and the associated shifts relative to the standards are then exported as an Excel file and used to calculate entrapment pressures.

Entrapment Pressure Calculations

To calculate entrapment pressures, the peak shifts between quartz inclusions and the Herkimer standards must be converted first to residual strain, then to average (current) pressure. Residual strain was quantified using the StRAinMAN software (Angel

et al., 2019), and the strain tensor was then converted to an average pressure (Pinc) (Gonzalez, Thomas, Baldwin, & Alvaro, 2019) using an Excel sheet provided by Mateo Alvaro (M. Kohn, personal communication, 2018). This newly calculated average pressure was then converted into the entrapment pressure (Ptrap) using garnet and quartz equations of state, as implemented with the EosFitPinc software (Angel et al., 2017). These Ptrap values can be displayed as an isomeke, which is a line that represents the potential entrapment across a specified temperature range. Maximum-pressure isomekes at garnet core, mantle, and rim locations were assumed to approximate the most likely entrapment conditions as these avoid potential biases such as re-equilibration of inclusions due to microfractures. Because assemblage modeling and inclusion thermobarometry were unable to constrain garnet nucleation P-T conditions based on chemistry, representative pressures for the garnet core, mantle, and (near) rim assume growth temperatures of 500, 550, and 600 °C respectively, derived from chemical inversion of FH-1M garnet zoning using simplified thermodynamics (Kohn, 2014b).

Electron Probe Microanalysis (EPMA):

Boise State University's Cameca SX5 EPMA was used to collect Mg, Mn, Fe, and Ca X-ray maps for garnets, quantitative chemical compositions on all minerals, and bulk rock chemical compositions. For all analyses, the accelerating voltage was set to 15 kV. For X-ray maps of garnet, the current was set at 200 nA and a beam size of 5-20 µm, depending on the size of the map. Complete chemical analyses used a current of 20 nA, a spot size of 1 µm for Fe-Mg minerals, and a spot size of 10 µm for white micas and plagioclase. Natural and synthetic silicates and oxides were used as standards. I also

collected quantitative spot analyses across the garnet and matrix minerals for calculations of bulk compositions.

Bulk compositions were calculated using 3 different methods. In method 1, I collected whole-thin-section X-ray maps to quantify proportions of minerals using the program, XMapTools (Lanari et al., 2014). XMapTools is a program that can help the user determine the modal abundance of minerals with section maps using a K-means statistical approach (Lanari et al., 2014). Knowing the compositions of the minerals from EPMA analysis, a bulk composition could be calculated. A second set of bulk compositions was collected by EDS analysis of a large region of each thick section using a defocused 40 μm electron beam. Using stage scanning, an area of 34x16mm was analyzed for FH1M and an area of 22x11.5mm was analyzed for Z3H. The bulk composition, from EDS spectra, was then calculated using the 'quant calculation' through the EDS software. Whole-rock compositions were calculated as follows: modal abundances for each mineral were used to determine the mass of the major weight percent oxides for each mineral. These individual masses were divided by the sum of all masses and multiplied by 100 to determine the bulk composition. A third bulk composition was calculated for FH-1M by collecting a grid of 130 spots and averaging.

The EDS bulk composition was used to calculate the core and rim P-T conditions for FH-1M. The XMapTools bulk composition was used to calculate the P-T conditions for Z3H because Theriak Domino and Perple_X could not calculate a MAD for the rim conditions with the bulk composition determined using EDS.

Multiple limitations could have prevented us from obtaining a reliable bulk composition from these rocks. First, we did not have sufficient physical sample of either

rock for XRF analysis. Having only thick sections to work with made it difficult to determine the heterogeneity in the layers where FH-1M and Z3H were located. It is also not always clear what scale of equilibrium is appropriate for calculating bulk compositions.

Mineral Assemblage Diagrams (MADs)

Mineral assemblage diagrams (MADs), also known as pseudosections, are P-T diagrams that display all of the stable mineral assemblages for a given isochemical system. MADs and chemical contour isopleths were calculated using two programs, Perple_X (Connolly, 2009) and Theriak Domino (de Capitani & Petrakakis, 2010) with the internally consistent HP98 and HP11 thermodynamic data sets (Holland & Powell, 1998, 2011) respectively for comparison.

The objective was to use a whole-rock bulk composition MAD with core composition isopleths to determine a core P-T condition, then use a garnet fractionated bulk composition MAD with rim composition isopleths to determine a rim P-T condition (Table A.2). Unfortunately, numerous amphibole and certain biotite models exceeded the computational abilities of the software or produced impossible compositions. Consequently, I ran multiple tests with different amphibole/biotite solution models (Table A.4). The models that succeeded in producing MADs and yielded the most reliable results in terms of likely mineral assemblages are presented in table A.4. Quartz and water were considered saturated phases in all of the MAD calculations. The models as calculated using Theriak Domino are presented in this paper.

Thermobarometry

Rim P-T conditions were calculated using rim and matrix mineral compositions with winTWQ v.2.32 (Berman, 1991), Thermocalc, AvePT (Powell & Holland, 1994), and GeoThermoBarometry ("GTB"; Spear & Kohn, 2006). For winTWQ, endmember components considered included almandine, annite, anorthite, eastonite, H_2O, kyanite, phlogopite, pyrope, quartz, siderophyllite, and staurolite. For AvePT, activities were calculated using program AX (Holland, 2019). Average P-T conditions were then calculated using Thermocalc v. ds62. Calculations with winTWQ were limited to the components almandine, annite, anorthite, eastonite, grossular, kyanite, phlogopite, pyrope, α-quartz, siderophyllite, staurolite (fixed activity = 0.77 based on Fe/Mg), and water. For GTB, thermometers included garnet-biotite (Berman, 1991; Ferry & Spear, 1978; garnet activity model), garnet-chlorite (Berman, 1991; Dickinson & Hewitt, 1986; garnet activity model), and garnet-hornblende (Graham & Powell, 1984); barometers included garnet-plagioclase-hornblende-quartz (Kohn & Spear, 1990) and garnet-plagioclase-kyanite-quartz (Koziol & Newton, 1988; Koziol, 1989).

Best Case Scenario Expectations

In principle, if the thermodynamic models and our estimated bulk compositions are accurate, minerals equilibrate rapidly on scales of centimeters, and QuiG and chemistry equivalently reflect entrapment conditions, we would expect the following:

- Core inclusion assemblages would match predicted assemblages for the whole rock composition (including garnet)
- The matrix assemblage would match predicted assemblages for the garnet-free whole rock composition

- Garnet compositional and zero molar isopleths would intersect at a unique P-T condition that is supported thermobarometrically—c. 600˚C and 7 kbar for the garnet rims (see results below) and lower temperatures and higher pressures for the garnet cores
- QuiG core isomekes would intersect garnet nucleation conditions inferred from whole-rock MADs
- QuiG rim isomekes would approach garnet rim P-T conditions inferred thermobarometrically and from garnet-free MADs

We recognize that variability in solution models will cause calculated MADs and P-T conditions to differ. The solution models we converged on for the MADs were those that allowed calculations at all and that most closely approximated observed assemblages. I did not attempt to optimize correspondence between P-T conditions calculated using MADs, thermobarometry, and QuiG.

RESULTS

Zoning Profiles and Thermobarometry

The garnets in FH-1M show decreases in Mn and Fe/(Fe+Mg), as well as increases in Mg towards the rim, which are consistent with the preservation of original garnet growth zoning (Figure 8). Plagioclase crystals in the FH-1M matrix show an increase in Ca towards the rim. The garnet in Z3H shows shallow compositional gradients except within ~100 μm of the rim, where Fe/(Fe+Mg), Mn, and Ca all decrease steeply (Figure 9). This rim region constitutes ~10% of the garnet by volume, and its zoning is also consistent with preservation of original garnet growth zoning. Plagioclase grains in the Z3H matrix are heterogenous across the peristerite gap with albite coexisting with oligoclase with maximum $X_{An} = 0.16$.

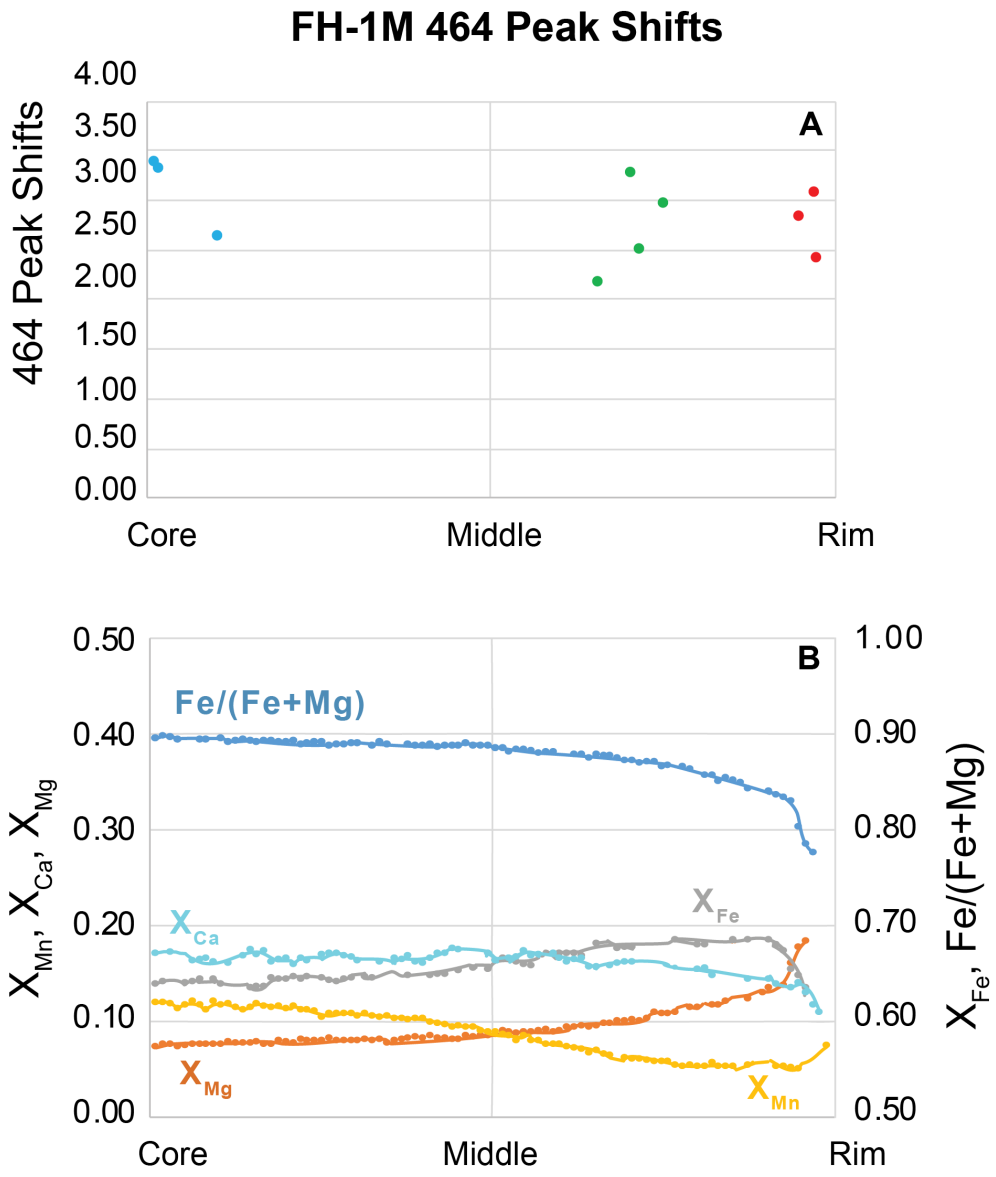

Figure 8. a) Shifts of the 464 cm^{-1} Raman peak of quartz inclusions relative to a standard vs. to their location in the FH-1M host garnet. Blue dots represent inclusions in the 'core', green dots represent inclusions in the 'middle', and red dots are inclusions located in the 'rim'. b) Core-to-rim zoning profile for Ca, Mg, Fe, Fe/(Fe + Mg), and Mn in FH-1M garnet. Traverse distance is ~7 mm.

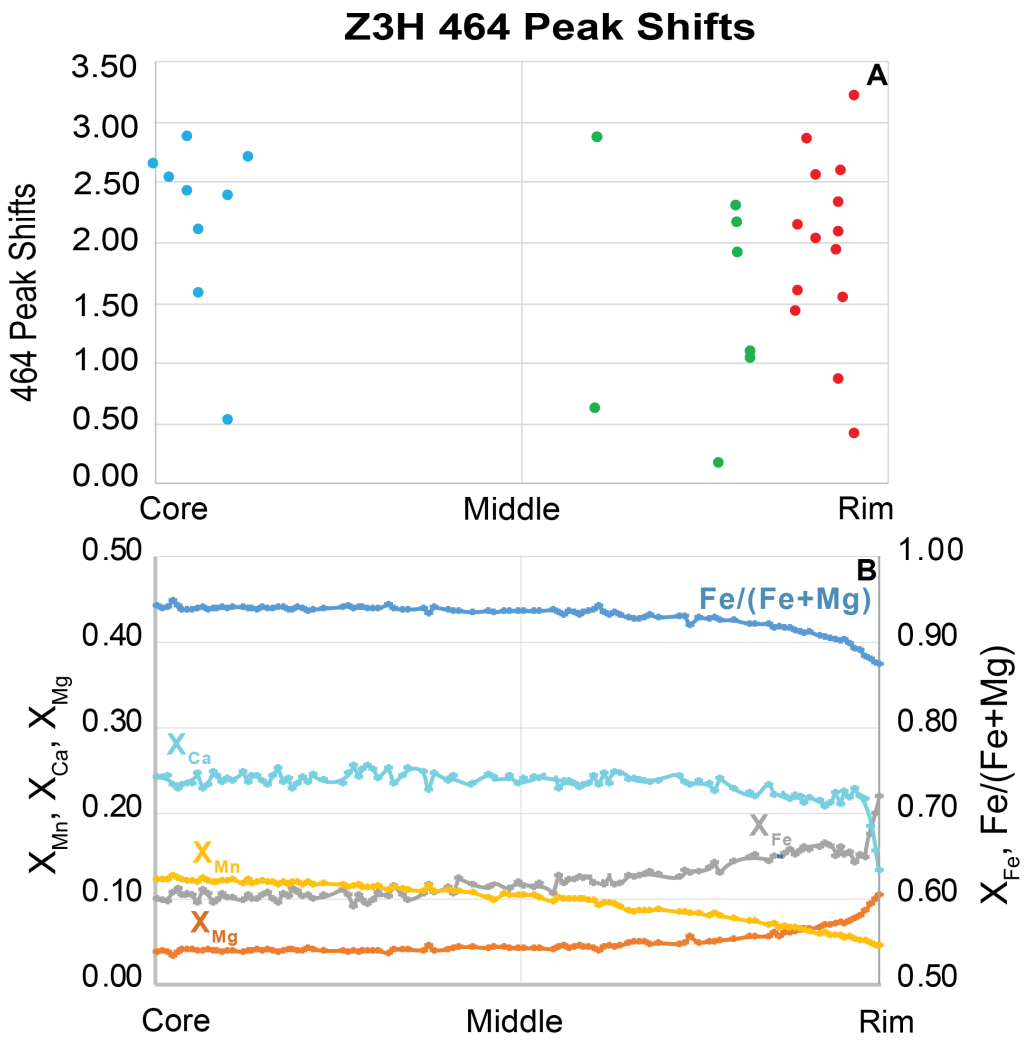

Figure 9. a.) Shifts of the 464 cm^{-1} Raman peak of quartz inclusions relative to a standard vs. their location in the Z3H host garnet. Blue dots represent inclusions in the 'core', green dots represent inclusions in the 'middle', and red dots are inclusions located in the 'rim'. b.) Core-to-rim zoning profile for Ca, Mg, Fe, Fe/(Fe + Mg), and Mn in Z3H garnet. Traverse distance is ~5 mm.

Conventional thermobarometry for FH-1M yields rim conditions of 635±25˚C and 7±1 kbar (Figure 10). For comparison with modeled MADs, a typical garnet core composition is X_{Grs} = 0.16 and X_{Alm} = 0.677 and a rim composition is X_{Grs} = 0.11 and X_{Alm} = 0.63; matrix biotite Fe/(Fe + Mg) = 0.78, and matrix plagioclase core is X_{An} = 0.28 and the rim composition is X_{An} = 0.33. The original P-T path calculated by Selverstone et al. (1984) involved a pressure decrease of c. 3 kbar during a temperature increase of c. 20 °C. A P-T path recalculated using updated (albeit simplified) thermodynamic properties (Kohn, 2014b) suggests a much more significant temperature change (c. 75 °C) over a similar pressure drop (~3.5 kbar).

Conventional thermobarometry for Z3H yields rim conditions of 575±25 °C and 7.5±0.5 kbar (Figure 11). For comparison with modeled MADs, a typical garnet core compision is X_{Grs} = 0.22 and X_{Alm} = 0.65 and a rim composition is X_{Grs} = 0.11 and X_{Alm} = 0.75; matrix biotite has Fe/(Fe + Mg) = 0.87. Matrix plagioclase in Z3H is peristeritic, with coexisting albite and oligoclase (X_{An} = 0.16).

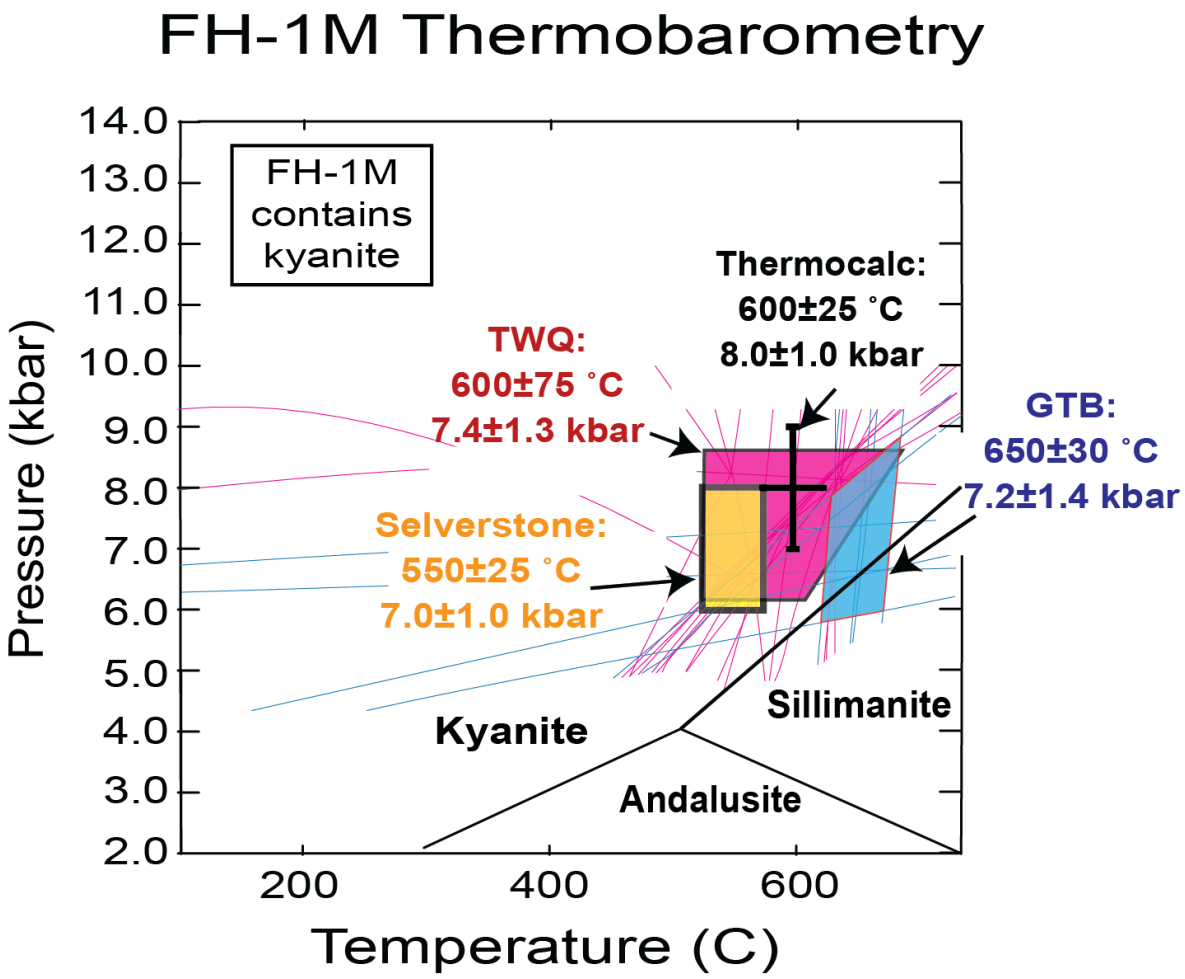

Figure 10. Rim thermobarometry for FH-1M showing close overlap among different methods. Colored lines represent specific equilibria calculated by winTWQ. The yellow shaded area from Selverstone et al. (1984) uses older thermobaromtetric calibrations and uses different matrix and rim compositions.

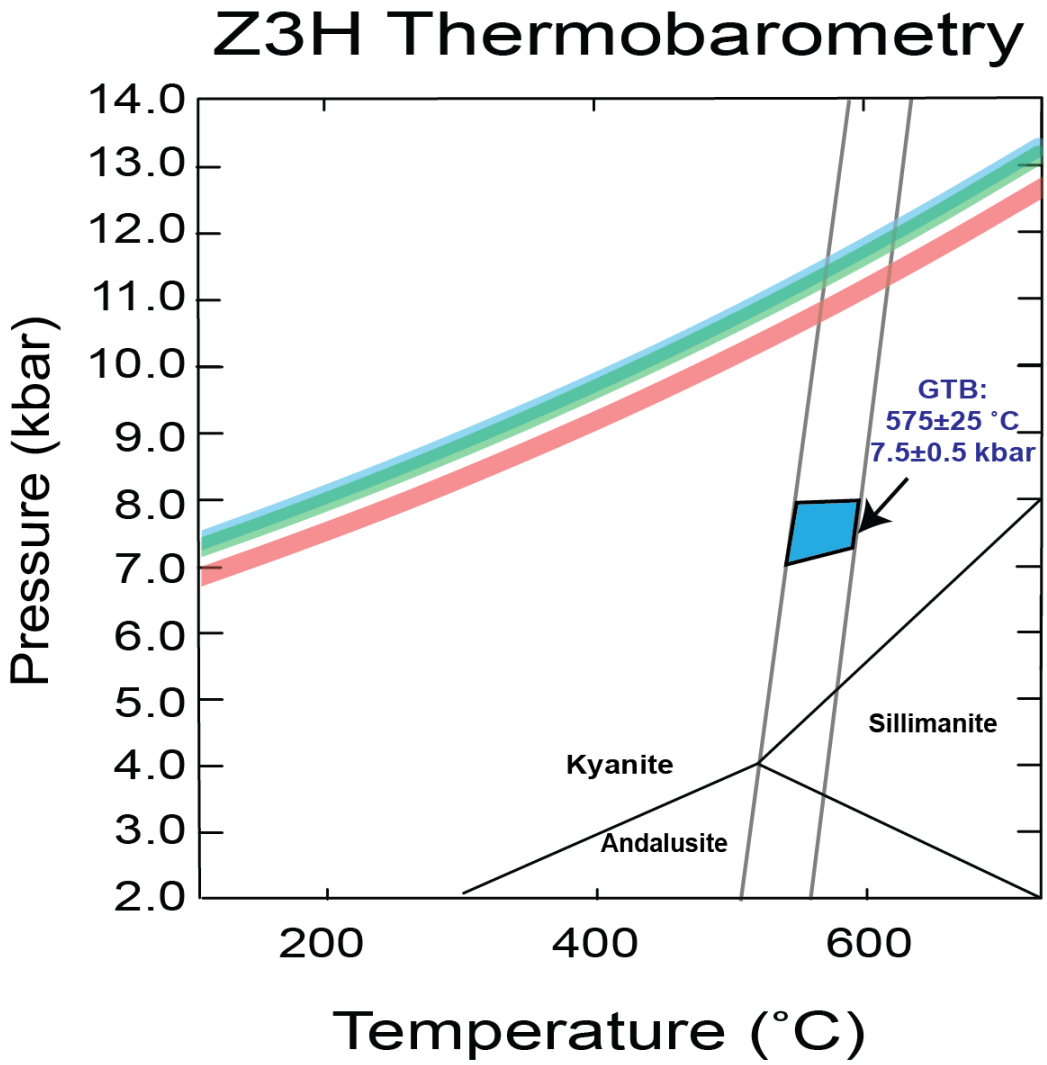

Figure 11. Rim thermobarometry for Z3H. The gray lines are the maximum and minimum thermometer lines. Maximum QuiG isomekes for Z3H core (blue), middle (green), and rim (red) quartz inclusions are shown as solid lines. The thickness of each isomeke represents its 300-bar analytical error.

QuiG

Maximum peak shifts in FH-1M inclusions (Figure 8 and Table A.5) imply QuiG isomekes that distribute towards lower pressure for core vs. mantle vs. rim at a constant temperature, or towards higher temperature at constant pressure. For example, at 550 °C, the calculated pressures would be 1.243 ± 0.032, 1.156±0.032, and 1.023±0.032 GPa for core, mantle, and rim (Figure 12). Errors represent propagated Raman peak (128, 206, and 464 cm^{-1}) uncertainties in measurement reproducibility. Depending on the likely temperature interval over which the garnet grew (e.g., 1 to 100 °C), QuiG barometry implies possible P-T paths ranging from isobaric heating to (nearly) isothermal exhumation. Maximum peak shifts in Z3H inclusions (Figure 9 and Table A.6) imply QuiG isomekes that are virtually indistinguishable for core vs. mantle. vs. rim. These imply a consistent pressure of ~11 kbar at 550 °C (Figure 12). However, there are no quartz inclusions in the outermost rim to compare with thermobarometry.

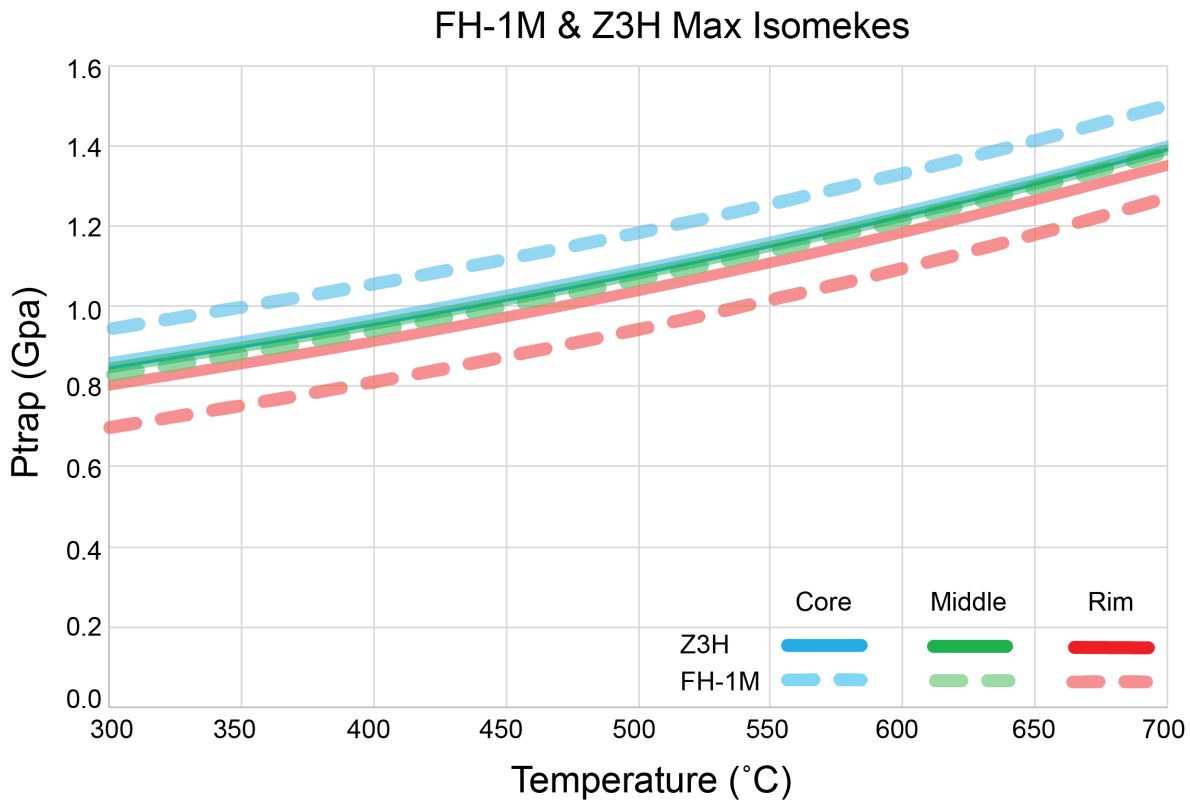

Figure 12. Maximum pressure QuiG isomekes for FH-1M (dashed lines) and Z3H (solid lines). Line thickness corresponds with analytical uncertainty (c. 300 bars for FH-1M and Z3H).

Mineral Assemblage Diagrams

A MAD for the measured FH-1M whole-rock composition and compositional isopleths for the garnet core imply garnet nucleation at ~580˚C and ~7 kbar in a stable assemblage of plagioclase-ilmenite-garnet-chlorite-biotite-clinoamphibole (Figure 13). Compositional isopleths for the FH1M rim in a garnet-free whole rock MAD intersect at 585˚C and 4 kbar with a predicted stable assemblage of plagioclase-ilmenite-garnet-biotite-clinoamphibole (Figure 14). No MAD predicts stable kyanite or staurolite, unlike the observed matrix mineral assemblage or the occurrence of kyanite and staurolite in numerous rocks in the region (Selverstone et al., 1984). Variations in a_{CO2} over a wide range of T at P=10 kbar also do not stabilize kyanite or staurolite. The implied core and rim P-T conditions deviate from the QuiG isomekes by several kbar (Figures 13-14).

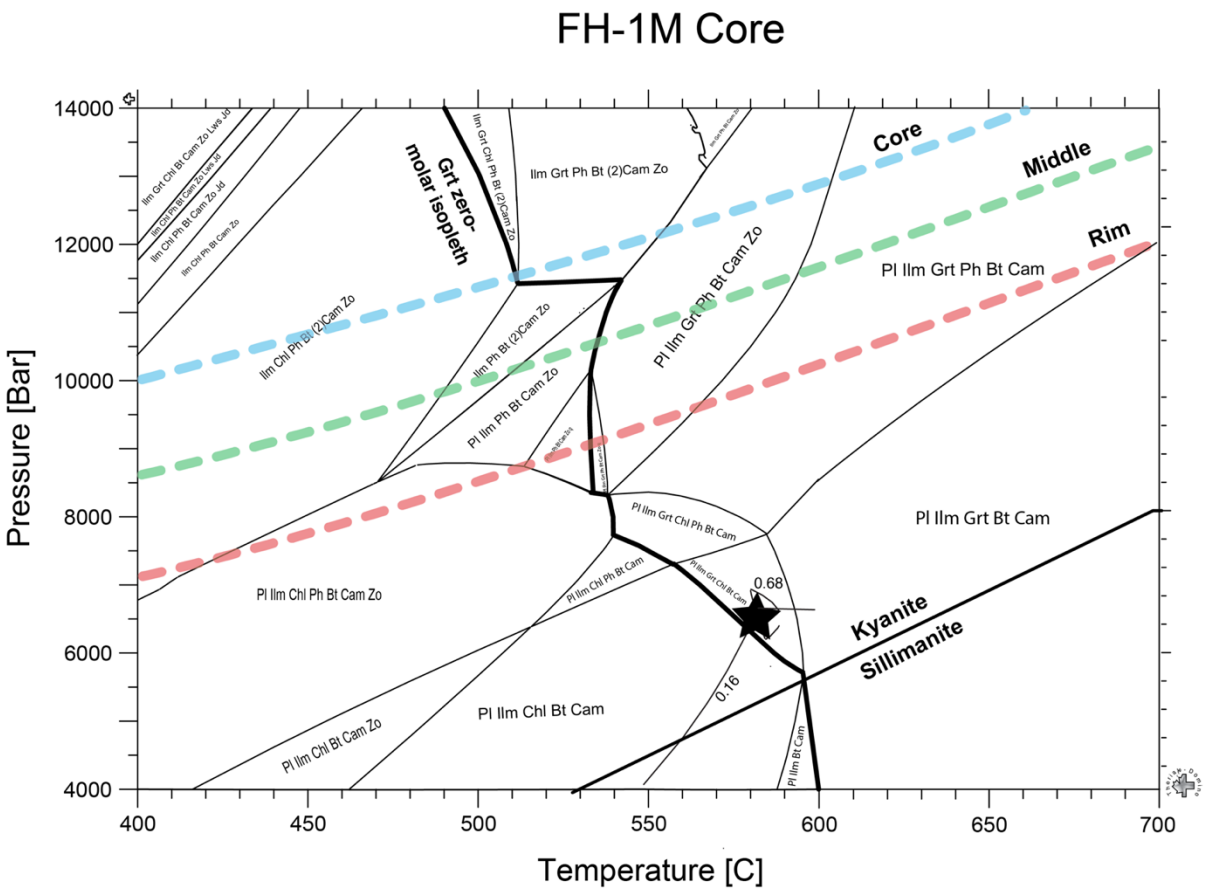

Figure 13. Mineral assemblage diagram for FH-1M whole rock (representative of FH-1M garnet nucleation) with maximum isomekes for FH-1M core (blue), middle (green), and rim (red) quartz inclusions. The thickness of each isomeke represents its 300-bar analytical error. Compositional isopleths for X_{Alm} (0.68) and X_{Grs} (0.16) intersect at ~580˚C and 6.5 kbar (black star), far from any isomeke.

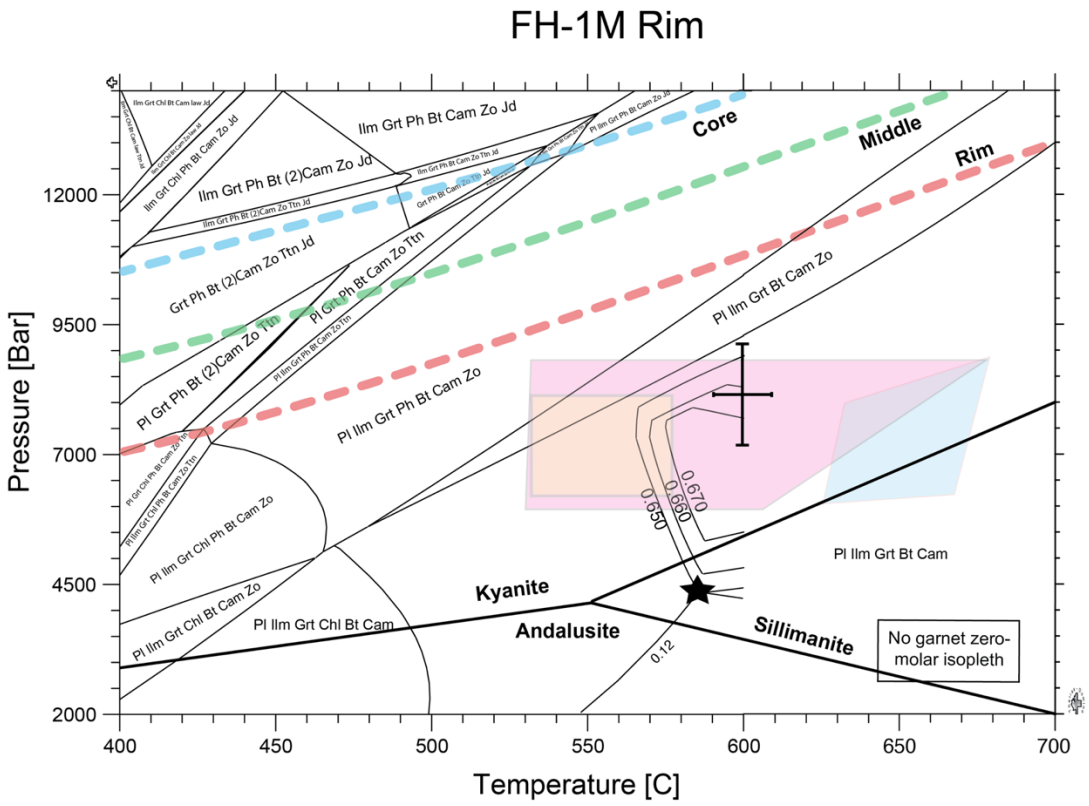

Figure 14. Mineral assemblage diagram for FH-1M garnet-free whole-rock (representative of FH-1M garnet rim) with maximum isomekes for FH-1M core (blue), middle (green), and rim (red) quartz inclusions. The thickness of each isomeke represents its 300-bar analytical error=. Compositional isopleths for X_{Alm} (0.65-0.67) and X_{Grs} (0.12) intersect at ~585˚C and 4.5 kbar (black star), several kbar below rim thermobarometric results. Colored boxes represent different thermobarometric methods. None of the assemblages predicted in this MAD corresponds with observations.

A MAD for the measured Z3H whole-rock composition or garnet-free composition did not have intersecting compositional isopleths (Figures 15-16). Rim thermobarometry for Z3H predicts a P-T condition of 575±25 °C and 7.5±0.5 kbar and a stable assemblage of plagioclase, garnet, chlorite, biotite, and 1-2 clinoamphiboles (Figure 16). The implied rim P-T condition deviate from the rim QuiG isomekes by several kbar (Figure 16).

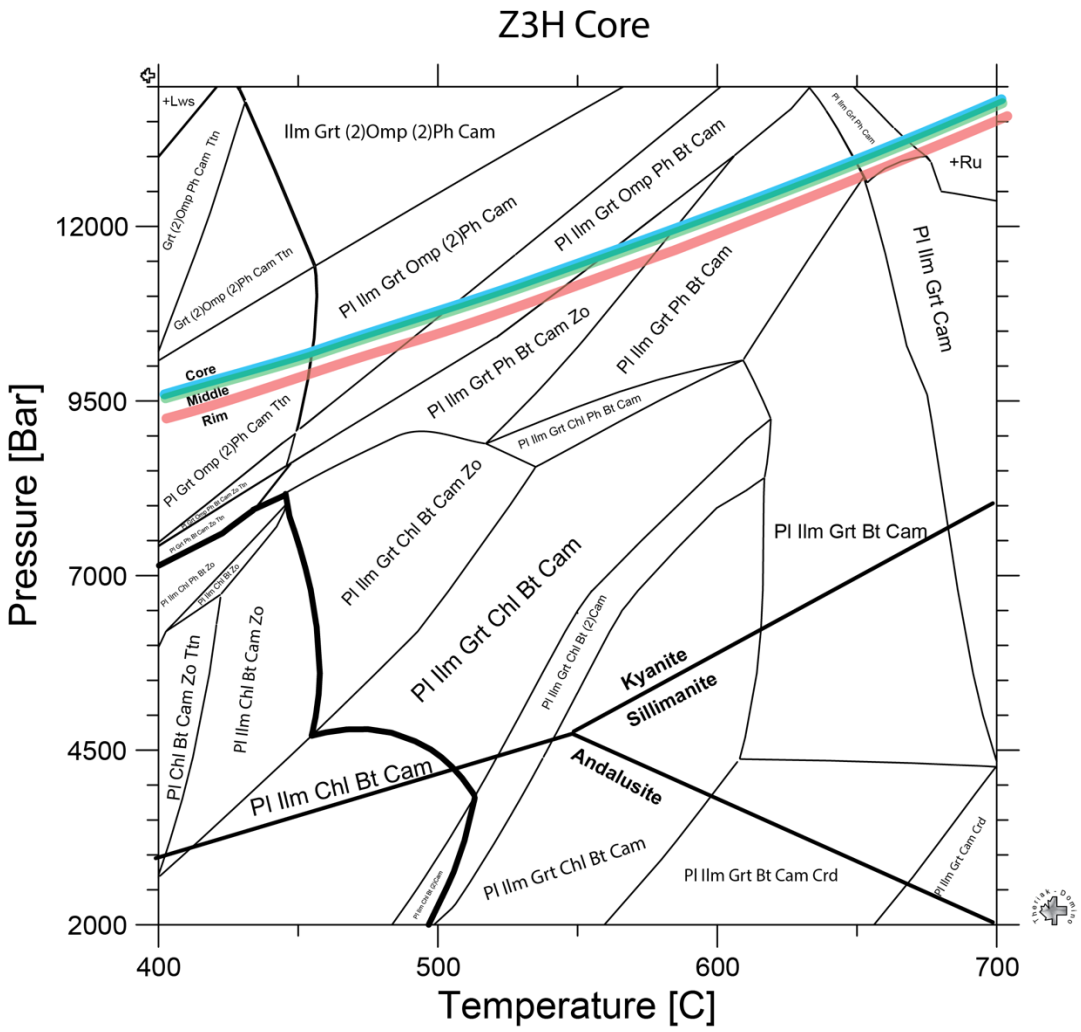

Figure 15. Mineral assemblage diagram for Z3H whole rock (representative of garnet core conditions) with maximum isomekes for Z3H core (blue), middle (green), and rim (red) quartz inclusions. The thickness of each isomeke represents its 300-bar analytical error. Compositional isopleths for X_{Alm} and X_{Grs} do not intersect. None of the assemblages predicted in this MAD corresponds with observations.

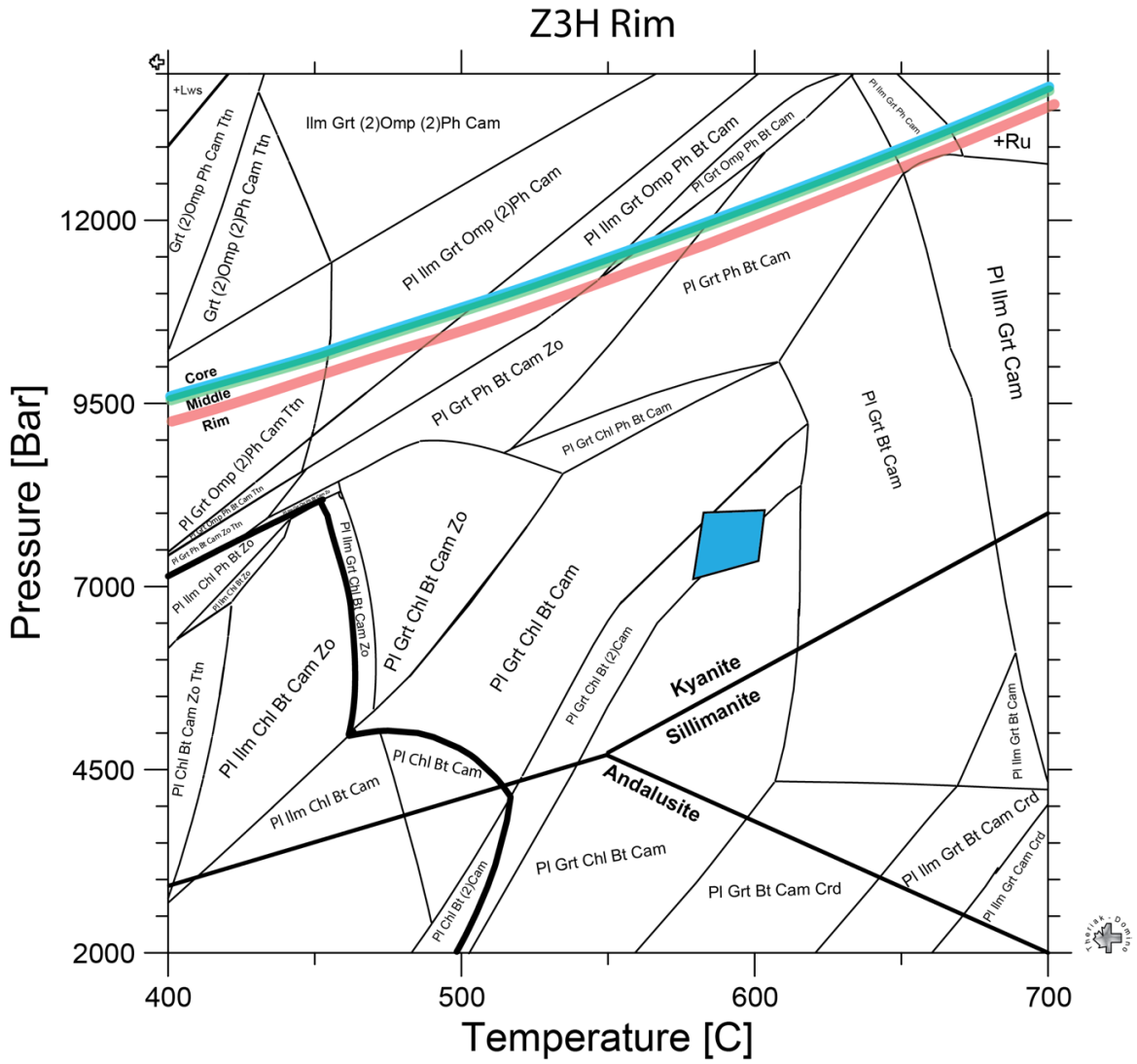

Figure 16. Mineral assemblage diagram for Z3H garnet-free whole-rock (representative of garnet rim conditions) with maximum isomekes for Z3H core (blue), middle (green), and rim (red) quartz inclusions. The thickness of each isomeke represents its 300-bar analytical error. Compositional isopleths for X_{Alm} and X_{Grs} do not intersect. None of the assemblages predicted in this MAD corresponds with observations.

DISCUSSION

Zoning Profiles & Thermobarometry

The relatively low peak temperatures (<650 °C), relatively large garnet diameters (1-2 cm), and relatively recent age of metamorphism (c. 35 Ma for the tectonically related USH; Selverstone, 1985) imply that diffusional modification was likely minimal. Garnet zoning generally shows patterns expected of prograde growth—decreasing Mn and Fe/(Fe+Mg) and increasing Mg from core to rim. The preservation of small oscillations in Mn also imply diffusional modification must have been minor. Consequently, we view garnet rim compositions paired with matrix mineral compositions to closely approximate peak conditions. Zoning in the FH-1M garnet is markedly steeper than in Z3H garnet. This might imply that much of the Z3H garnet grew with only small changes in pressure and temperature.

FH-1M rim P-T conditions are 635±25˚C, 7±1 kbar vs. 550±25˚C and 7±1 kbar published by Selverstone et al. (1984). The differences in apparent temperatures mainly reflect more complete characterization of garnet and biotite chemical variability. More specifically, garnet rim compositions are more Mg-rich and biotite compositions are more Fe-rich than originally inferred. Conventional thermobarometry for the Z3H rim (575±25 °C, 7.5±0.5 kbar) yields a lower temperature, but similar pressure to FH-1M. Selverstone et al. (1984) calculated different P-T conditions for garnet cores based on plagioclase inclusion compositions. These calculations assumed that kyanite was stable throughout garnet growth, but kyanite inclusions do not appear in garnet. Core P-T conditions calculated by Selverstone et al. (1984) were 530 °C and 10 kbar, implying a relatively

significant decrease in pressure (3 kbar) with a slight increase in temperature (20 °C). A P-T path for FH-1M, recalculated using the Gibbs method with updated (albeit simplified) thermodynamic properties, has suggested a much more significant temperature change (c. 75 °C) over a similar pressure drop (~3.5 kbar; Kohn, 2014b). Whereas rim P-T conditions are consistent between our study and previous work in the LSH (Droop, 1985; Selverstone et al., 1984), we cannot independently assess the accuracy of calculated core P-T conditions using thermobarometry for either rock because they lack appropriate inclusion assemblages and compositions.

Consistency of QuiG with the Selverstone et al. (1984) P-T Path

If we assume that both garnets nucleated at a similar temperature of ~500˚C (a reference temperature based on the recalculated P-T path for FH-1M; Kohn, 2014b), both samples imply nucleation at the same pressure of ~11kbar. This pressure is slightly higher than predicted by modeling of FH-1M (Kohn, 2014b; Selverstone et al., 1984), but is broadly consistent with the interpretation that the cores nucleated at a higher pressure than the rims. QuiG isomekes in both samples plot towards higher temperature or lower pressure approaching the rims of the garnets. This is broadly consistent with growth of garnet during exhumation with heating as originally proposed by Selverstone et al. (1984). However, the QuiG isomekes for Z3H tightly cluster throughout the volume of garnet analyzed (c. 90%). This implies that 90% or more of the Z3H garnet grew over small changes in pressure and temperatures or along a QuiG isomeke (heating with a slight increase in pressure). The P-T path calculation of Selverstone et al. (1984) does imply a small increase in pressure and temperature during initial garnet growth, but the overall sense of the P-T path is dominated by exhumation, not loading. Consequently, we

infer that growth of about 90% of the Z3H garnet occurred at nearly constant pressure and temperature. QuiG isomekes for inclusions as close to the rims of the garnets as possible imply pressures for late stage garnet growth that are considerably higher than pressures determined thermobarometrically. This disparity could reflect additional exhumation during the latest garnet growth that is captured in chemical zoning and rim compositions where QuiG barometry is not possible. The strong chemical zoning in Z3H is consistent with large changes in pressure/temperature during the last (~10%) growth of the garnet.

Overall, we can generally reconcile QuiG results with the P-T path of Selverstone et al. (1984; as recalculated by Kohn, 2014b), but doing so implies the following: First, nearly all the Z3H garnet grew at nearly constant P-T conditions. The exhumation path would then be recorded (if at all) only in the outermost zoning. Second, whereas FH-1M does record some exhumation via QuiG, the largest decrease in pressure was not captured by quartz inclusions. Because moderate pressure quartz inclusions were entrapped very close to the end of garnet growth, the exhumation path would again be recorded only in the outermost zoning.

MADs

Despite our attempts to optimize calculations, many predictions of the MADs differ from observations in our rocks. For the garnet-free FH-1M whole rock composition (effectively modeling the current matrix assemblages and garnet rim compositions), the predicted peak assemblage lacks staurolite, kyanite, and paragonite, a zero garnet molar isopleth does not exist, and garnet compositional isopleths do not intersect with thermobarometrically determined P-T conditions. Staurolite in FH-1M appears embayed

and anhedral, so may not be part of the stable peak assemblage. However, kyanite appears prismatic with no prominent reaction features. Textural evidence supports mutual equilibrium among kyanite, staurolite, and hornblende in many rocks collected by Selverstone et al. (1984). For the FH-1M whole rock composition (effectively modeling assemblages and garnet core compositions at the point where garnet nucleated), although garnet molar and compositional isopleths do intersect at a P-T condition of ~6 kbar and 575˚C, predicted plagioclase composition (~An_{40}) differs from plagioclase inclusion and matrix core compositions (<An_{30}). If a core pressure of c. 10-12 kbar is assumed, based on QuiG barometry and Selverstone et al. (1984), phengite is predicted in the stable assemblage, but is never observed as an inclusion. These disparities between predictions and observations caution against interpreting P-T conditions from these specific MADs.

For Z3H rim (garnet-free whole-rock), the predicted peak assemblage lacks a second plagioclase and ilmenite, and there is no region that predicts cummingtonite. Further, the garnet zero molar isopleth is predicted at an unrealistically low P-T condition. For Z3H core, the predicted assemblage at an assumed P-T condition of ~10-12 kbar and ~500˚C contains phengite, paragonite, and omphacite, which were not found as inclusions.

Overall, the unusual bulk compositions of our rocks defy accurate modeling. Although we cannot rule out disequilibrium, this failure seems likely to reflect poorly constrained thermodynamic properties or solution models. The sensitivity of the MADs to amphibole and biotite solution models suggests these two minerals as likely sources of error.

What is the correct P-T path?

If thermodynamic models, thermobarometry, and QuiG barometry all yield different results, how can we know what the P-T path was for these samples? The internal consistency among calculated rim P-T conditions across multiple samples of differing composition (Droop, 1985; Selverstone et al., 1984; this study) suggests a final P-T condition of ~600˚C and 7 kbar is likely robust. The increase in X_{Grs}/X_{An} for plagioclase inclusions in garnet cores, combined with consistent QuiG results, strongly suggests garnet cores nucleated at higher pressures. Although we cannot directly infer garnet nucleation temperatures, a "clockwise" P-T path (exhumation with heating) is likely correct. We are unable to reproduce the calculations of Selverstone et al. (1984) partly because the bulk compositions are not amendable to modeling, but also because we do not know how assemblages might have changed during garnet growth. Selverstone et al. (1984) assumed that garnet grew entirely in an assemblage represented by matrix minerals. But, for example, we find no inclusions of staurolite or kyanite in FH-1M. Still, although we cannot directly reproduce the calculations of Selverstone et al. (1984), the overall path and tectonic interpretations appear robust.

Was there garnet overstepping?

The MADs appear too sensitive to thermodynamic uncertainties to provide reliable nucleation conditions. However, the QuiG results for Z3H could support nucleation overstepping. The QuiG isomekes for Z3H garnet show very little change from core to rim. This, along with shallow zoning profiles could support rapid, isobaric-isothermal growth, as predicted for overstepped garnet growth (Pattison & Tinkham, 2009; Pattison et al., 2011; Spear, 2017; Spear et al., 2014). However, the actual shape of

garnet zoning profiles should not be used to determine if a garnet has nucleated due to overstepping (Spear, 2017; Spear & Wolfe, 2018, 2020). Furthermore, the Z3H garnet has abundant quartz inclusions from core to rim (except for the outermost rim). Possibly, textures proxy for growth kinetics, such that abundant inclusions represent overstepping while sparse inclusions represent slow, post-overstepping equilibrium growth as temperature increased (F. Spear, personal communication, 2019).

CONCLUSIONS AND FUTURE DIRECTIONS

Current MADs do not reproduce either the results of Selvserstone et al. (1984) or petrologic observations such as mineral assemblages and likely P-T conditions as determined using independent thermobarometers. We interpret these inconsistencies to suggest that current thermodynamic models are not robust for rocks of this bulk composition and need to be updated.

While some rocks show good correspondence between QuiG barometry and P-T conditions calculated using garnet zoning or conventional thermobarometry, other rocks do not (Spear & Wolfe, 2020). For example, Spear and Wolfe (2020) found that QuiG-derived pressures for rocks from the Orfordville Belt, New Hampshire (Spear & Rumble, 1986), Townshend Dam, Vermont (Dragovic et al., 2018; Kohn & Valley, 1994), the Connecticut Valley Trough, Vermont (Wolfe & Spear, 2018) and Sifnos, Greece (Castro & Spear, 2017) differed from pressures inferred using garnet chemical zoning. For example, Castro and Spear (2017) inferred significant overstepping (1.2-1.4 GPa) of the garnet isograd.

These inconsistencies pose the question about the reliability of QuiG barometry vs. thermodynamic calculations of P-T conditions, especially regarding the accuracy of P-T conditions of garnet nucleation and growth. Numerous studies use traditional thermodynamic methods, such as garnet chemical zoning, to determine P-T paths. If results from QuiG barometry are correct, studies that invert garnet chemical zoning for P-T evolution need to be reevaluated. My QuiG results may question the P-T constraints

determined by Selverstone et al. (1984), but overall imply a similar P-T path and tectonic interpretations. Further comparison of the internal consistency among thermodynamic models and QuiG may show how thermodynamic solution models can be improved.

REFERENCES

Ackermand, D., & Raase, P. (1978). Metamorphism of the Penninic Series in the western Tauern Window (Austria/Italy). *Interunion Kommission on Geodynamics, 38*, 121-124.

Al-Rumaithi, A. (2020). Raman spectrum baseline removal. Retrieved September 8, 2020, from https://www.mathworks.com/matlabcentral/fileexchange/69649-raman-spectrum-baseline-removal

Angel, R. J., Mazzucchelli, M. L., Alvaro, M., & Nestola, F. (2017). EosFit-Pinc: A simple GUI For host-inclusion elastic thermobarometry. *American Mineralogist, 102*(9), 1957-1960. doi:10.2138/am-2017-6190

Angel, R. J., Mazzucchelli, M. L., Alvaro, M., Nimis, P., & Nestola, F. (2014). Geobarometry from host-inclusion systems: The role of elastic relaxation. *American Mineralogist, 99*(10), 2146-2149. doi:10.2138/am-2014-5047

Angel, R. J., Murri, M., Mihailova, B., & Alvaro, M. (2019). Stress, strain and Raman shifts. *Zeitschrift Für Kristallographie - Crystalline Materials, 234*(2), 129-140. doi:10.1515/zkri-2018-2112

Ashley, K. T., Steele-MacInnis, M., & Caddick, M. J. (2014). QuIB calc: A MATLAB® script for geobarometry based on Raman spectroscopy and elastic modeling of quartz inclusions in garnet. *Computers & Geosciences, 66*, 155-157. doi:10.1016/j.cageo.2014.01.005

Berman, R. G. (1991). Thermobarometry using multi-equilibrium calculations; a new technique, with petrological applications. *The Canadian Mineralogist, 29*(4), 833-855.

Campomenosi, N., Mazzucchelli, M. L., Mihailova, B., Scambelluri, M., Angel, R. J., Nestola, F., . . . Alvaro, M. (2018). How geometry and anisotropy affect residual strain in host-inclusion systems: Coupling experimental and numerical approaches. *American Mineralogist, 103*(12), 2032-2035. doi:10.2138/am-2018-6700ccby

Castro, A. E., & Spear, F. S. (2017). Reaction overstepping and re-evaluation of peak P–T conditions of the blueschist unit Sifnos, Greece: Implications for the Cyclades subduction zone. *International Geology Review, 59*, 548-562. doi:10.1080/00206814.2016.1200499

Cizina, M. F. (2020). *Optimizing Raman spectral collection for quartz and zircon crystals for elastic geothermobarometry* (Unpublished master's thesis). Boise State University.

Cliff, R. A. (1981). Pre-Alpine history of the Pennine zone in The Tauern Window, Austria: U-PB And Rb-Sr geochronology. *Contributions to Mineralogy and Petrology, 77*(3), 262-266. doi:10.1007/bf00373541

Connolly, J. A. (2009). The geodynamic equation of state: What and how. *Geochemistry, Geophysics, Geosystems,10*(10). doi:10.1029/2009gc002540

Dale, J., Holland, T., & Powell, R. (2000). Hornblende-garnet-plagioclase thermobarometry: A natural assemblage calibration of the thermodynamics of hornblende. *Contributions to Mineralogy and Petrology*, *140*(3), 353–362. https://doi.org/10.1007/s004100000187

Dickenson, M., III, & Hewitt, D. (n.d.). A garnet-chlorite geothermometer [Abstract]. *Geological Society of America Abstracts Program*.

De Capitani, C., & Petrakakis, K. (2010). The computation of Equilibrium Assemblage diagrams with Theriak/domino software. *American Mineralogist, 95*(7), 1006-1016. doi:10.2138/am.2010.3354

Dragovic, B., Gatewood, M. P., Baxter, E. F., & Stowell, H. H. (2018). Fluid production rate during the regional metamorphism of a pelitic schist. *Contributions to Mineralogy and Petrology, 173*(11). doi:10.1007/s00410-018-1523-9

Droop, G. T. (1985). Alpine metamorphism in the south-east Tauern Window, Austria: 1. P-T variations in space and time. *Journal of Metamorphic Geology, 3*(4), 371-402. doi:10.1111/j.1525-1314.1985.tb00326.x

Enami, M., Nishiyama, T., & Mouri, T. (2007). Laser Raman microspectrometry of metamorphic quartz: A simple method for comparison of metamorphic pressures. *American Mineralogist, 92*(8-9), 1303-1315. doi:10.2138/am.2007.2438

Ferry, J. M., & Spear, F. S. (1978). Experimental calibration of the partitioning of Fe and Mg Between biotite and garnet. *Contributions to Mineralogy and Petrology, 66*(2), 113-117. doi:10.1007/bf00372150

Franzolin, E., Schmidt, M. W., & Poli, S. (2011). Ternary Ca–Fe–Mg carbonates: subsolidus phase relations at 3.5 gpa and a thermodynamic solid solution model including order/disorder. *Contributions to Mineralogy and Petrology, 161*(2), 213-227. doi:10.1007/s00410-010-0527-x

Fuhrman, M. L., & Lindsley, D. H. (1988). Ternary-feldspar modeling and thermometry. *American Mineralogist, 73*, 201-215.

Gonzalez, J. P., Thomas, J. B., Baldwin, S. L., & Alvaro, M. (2019). Quartz-in-garnet and Ti-in-quartz thermobarometry: Methodology and first application to a quartzofeldspathic gneiss from Eastern Papua New Guinea. *Journal of Metamorphic Geology, 37*(9), 1193-1208. doi:10.1111/jmg.12508

Graham, C. M., & Powell, R. (1984). A garnet-hornblende geothermometer: Calibration, testing, and application to the Pelona Schist, Southern California. *Journal of Metamorphic Geology, 2*(1), 13-31. doi:10.1111/j.1525-1314.1984.tb00282.x

Green, E. C., Holland, T. J., & Powell, R. (2007). An order-disorder model for omphacitic pyroxenes in the system jadeite-diopside-hedenbergite-acmite, with applications to eclogitic rocks. *American Mineralogist, 92*(7), 1181-1189. doi:10.2138/am.2007.2401

Green, E. C., White, R. W., Diener, J. F., Powell, R., Holland, T. J., & Palin, R. M. (2016). Activity-composition relations for the calculation of partial melting equilibria in metabasic rocks. *Journal of Metamorphic Geology, 34*(9), 845-869. doi:10.1111/jmg.12211

Groß, P., Pleuger, J., Handy, M. R., Germer, M., & John, T. (2020). Evolving temperature field in a fossil subduction channel during the transition from subduction to collision (Tauern Window, Eastern Alps). *Journal of Metamorphic Geology, 39*(2), 247-269. doi:10.1111/jmg.12572

Holland, T. (2019, October). AX : Calculate activities of mineral endmembers from chemical analyses. Retrieved June 15, 2021, from https://filedn.com/lU1GlyFhv3UuXg5E9dbnWFF/TJBHpages/ax.html

Holland, T. J., & Powell, R. (1998). An internally consistent thermodynamic data set for phases of petrological interest. *Journal of Metamorphic Geology, 16*, 309-343. doi:10.1111/j.1525-1314.1998.00140.x

Holland, T. J., & Powell, R. (2011). An improved and extended internally consistent thermodynamic dataset for phases of petrological interest, involving a new equation of state for solids. *Journal of Metamorphic Geology, 29*(3), 333-383. doi:10.1111/j.1525-1314.2010.00923.x

Horváth, F., Bada, G., Szafián, P., Tari, G., Ádám, A., & Cloetingh, S. (2006). Formation and deformation of the Pannonian basin: Constraints from observational data. *Geological Society, London, Memoirs, 32*(1), 191-206. doi:10.1144/gsl.mem.2006.032.01.11

Kohn, M. J., & Spear, F. S. (1990). Two new geobarometers for garnet amphibolites, with applications to southeastern Vermont. *American Mineralogist, 75*, 89-96.

Kohn, M. J., & Valley, J. W. (1994). Oxygen isotope constraints on metamorpihc fluid flow, Townshend Dam, Vermont, U.S.A. *Geochimica Et Cosmochimica Acta, 58*(24), 5551-5566. doi:10.1016/0016-7037(94)90249-6

Kohn, M. J. (2014a). “Thermoba-Raman-try”: Calibration of spectroscopic barometers and thermometers for mineral inclusions. *Earth and Planetary Science Letters, 388*, 187-196. doi:10.1016/j.epsl.2013.11.054

Kohn, M. J. (2014b). Geochemical zoning in metamorphic minerals. *Treatise on Geochemistry,* 249-280. doi:10.1016/b978-0-08-095975-7.00307-7

Koziol, A. M., & Newton, R. C. (1988). Redetermination of the anorthite breakdown reaction and improvement of the plagioclase-garnet-Al2SiO5 aquartz geobarometer. *American Mineralogist, 7*(3), 216-223.

Koziol, A. M. (1989). Recalibration of the gamet-plagioclase-Al2SiO5-quartz (GASP) geobarometer and applications for natural parageneses. *EOS, 70*, 493.

Lanari, P., Vidal, O., De Andrade, V., Dubacq, B., Lewin, E., Grosch, E. G., & Schwartz, S. (2014). XMapTools: A MATLAB©-based program for electron Microprobe x-ray image processing And geothermobarometry. *Computers & Geosciences, 62*, 227-240. doi:10.1016/j.cageo.2013.08.010

Linzer, H., Decker, K., Peresson, H., Dell'Mour, R., & Frisch, W. (2002). Balancing lateral orogenic float of the Eastern Alps. *Tectonophysics, 354*(3-4), 211-237. doi:10.1016/s0040-1951(02)00337-2

Lippitsch, R., Kissling, E., & Ansorge, J. (2003). Upper mantle structure beneath the Alpine orogen from high-resolution teleseismic tomography. *Journal of Geophysical Research, 108*(B8). doi:10.1029/2002jb002016

Mazzucchelli, M., Burnley, P., Angel, R., Morganti, S., Domeneghetti, M., Nestola, F., & Alvaro, M. (2018). Elastic geothermobarometry: Corrections for the geometry of the host-inclusion system. *Geology, 46*(3), 231-234. doi:10.1130/g39807.1

Morteani, G., & Raase, P. (1974). Metamorphic plagioclase crystallization and zones of equal anorthite content in epidote-bearing, amphibole-free rocks of the Western Tauernfenster, Eastern Alps. *Lithos, 7*(2), 101-111. doi:10.1016/0024-4937(74)90023-1

Murri, M., Mazzucchelli, M. L., Campomenosi, N., Korsakov, A. V., Prencipe, M., Mihailova, B. D., . . . Alvaro, M. (2018). Raman elastic geobarometry for anisotropic mineral inclusions. *American Mineralogist, 103*, 1869-1872. doi:10.2138/am-2018-6625ccby

Pattison, D. R., & Tinkham, D. K. (2009). Interplay between equilibrium and kinetics in prograde metamorphism of pelites: An example from the Nelson Aureole, British Columbia. *Journal of Metamorphic Geology, 27*(4), 249-279. doi:10.1111/j.1525-1314.2009.00816.x

Pattison, D. R. M., de Capitani, C., & Gaidies, F. (2011). Petrological consequences of variations in metamorphic reaction affinity. *Journal of Metamorphic Geology*, *29*(9), 953–977. https://doi.org/10.1111/j.1525-1314.2011.00950.x

Raith, M., Hormann, P. K., & Abraham, K., 1977. Petrology and metamorphic evolution of the Penninic ophiolites in the western Tauern Window (Austria). *Schweiz. miner.petrogr. Mitt. 57*, 187-232.

Ratschbacher, L., Frisch, W., Linzer, H., & Merle, O. (1991). Lateral extrusion in the Eastern Alps, Part 2: Structural analysis. *Tectonics, 10*(2), 257-271. doi:10.1029/90tc02623

Rosenberg, C. L., Brun, J., Cagnard, F., & Gapais, D. (2007). Oblique indentation in the Eastern Alps: Insights from laboratory experiments. *Tectonics, 26*(2). doi:10.1029/2006tc001960

Rosenfeld, J. L., & Chase, A. B. (1961). Pressure and temperature of crystallization from elastic effects around solid inclusions in minerals? *American Journal of Science, 259*(7), 519-541. doi:10.2475/ajs.259.7.519

Sander, B. (1911).: Geologische Studien am Westende der Hohen Tauern. I. *Bericht. Denkschr. d. kais. Akad. d. Wiss. Wien 83*, 257–319.

Scharf, A., Handy, M. R., Favaro, S., Schmid, S. M., & Bertrand, A. (2013). Modes of orogen-parallel stretching and extensional exhumation in response to microplate indentation and roll-back subduction (Tauern Window, Eastern Alps). *International Journal of Earth Sciences, 102*(6), 1627-1654. doi:10.1007/s00531-013-0894-4

Schmid, S. M., Scharf, A., Handy, M. R., & Rosenberg, C. L. (2013). The Tauern Window (Eastern Alps, Austria): A new tectonic map, with cross-sections and a tectonometamorphic synthesis. *Swiss Journal of Geosciences, 106*(1), 1-32. doi:10.1007/s00015-013-0123-y

Selverstone, J., & Spear, F. S. (1985). Metamorphic P-T paths from pelitic schists and greenstones from the south-west Tauern Window, Eastern Alps. *Journal of Metamorphic Geology, 3*(4), 439-465. doi:10.1111/j.1525-1314.1985.tb00329.x

Selverstone, J., Spear, F. S., Franz, G., & Morteani, G. (1984). High-Pressure metamorphism in the SW Tauern Window, Austria: P-T paths from hornblende-kyanite-staurolite schists. *Journal of Petrology, 25*(2), 501-531. doi:10.1093/petrology/25.2.501

Selverstone, J. (1985). Petrologic constraints on imbrication, metamorphism, and uplift in the SW Tauern Window, Eastern Alps. *Tectonics, 4*(7), 687-704. doi:10.1029/tc004i007p00687

Smye, A. J., Greenwood, L. V., & Holland, T. J. (2010). Garnet-chloritoid-kyanite assemblages: Eclogite facies indicators of subduction constraints in orogenic belts. *Journal of Metamorphic Geology, 28*(7), 753-768. doi:10.1111/j.1525-1314.2010.00889.x

Spear, F. S. (2017). Garnet growth after overstepping. *Chemical Geology, 466*, 491-499. doi:10.1016/j.chemgeo.2017.06.038

Spear, F. S., & Kohn, M. J. (2006, March 30). Metamorphic petrology at RPI. Retrieved from http://ees2.geo.rpi.edu/MetaPetaRen/Software/GTB_Prog/GTB.html

Spear, F. S., & Rumble, D. (1986). Pressure, temperature, and structural evolution of the Orfordville Belt, west-central New Hampshire. *Journal of Petrology, 27*(5), 1071-1093. doi:10.1093/petrology/27.5.1071

Spear, F. S., & Selverstone, J. (1983). Quantitative P-T paths from zoned minerals: Theory and tectonic applications. *Contributions to Mineralogy and Petrology*, *83*(3–4), 348–357. https://doi.org/10.1007/BF00371203

Spear, F. S., & Wolfe, O. M. (2018). Evaluation of the effective bulk composition (EBC) during growth of garnet. *Chemical Geology, 491*, 39-47. doi:10.1016/j.chemgeo.2018.05.019

Spear, F. S., & Wolfe, O. M. (2020). Revaluation of "equilibrium" P-T paths from zoned garnet in light of quartz inclusion in garnet (QuiG) barometry. *Lithos, 372-373*, 1-10. doi:10.1016/j.lithos.2020.105650

Spear, F. S., Selverstone, J., Hickmott, D., Crowley, P., & Hodges, K. V. (1984). P-T paths from garnet zoning: A new technique for deciphering tectonic processes in crystalline terranes. *Geology, 12*(2), 87-90. doi:10.1130/0091-7613(1984)122.0.co;2

Spear, F. S., Thomas, J. B., & Hallett, B. W. (2014). Overstepping the garnet isograd: A comparison of QuiG barometry and thermodynamic modeling. *Contributions to Mineralogy and Petrology, 168*(3). doi:10.1007/s00410-014-1059-6

White, R. W., Pomroy, N. E., & Powell, R. (2005). An in situ metatexite-diatexite transition in upper amphibolite facies rocks from Broken Hill, Australia. *Journal of Metamorphic Geology, 23*(7), 579-602. doi:10.1111/j.1525-1314.2005.00597.x

White, R. W., Powell, R., & Johnson, T. E. (2014). The effect of Mn on mineral stability in metapelites revisited: New a -X relations for manganese-bearing minerals. *Journal of Metamorphic Geology, 32*(8), 809-828. doi:10.1111/jmg.12095

Wolfe, O. M., & Spear, F. S. (2018). Determining the amount of overstepping required to nucleate garnet during Barrovian regional metamorphism, Connecticut Valley Synclinorium. *Journal of Metamorphic Geology, 36*(1), 79-94. doi:10.1111/jmg.12284

Zhang, Y. (1998). Mechanical and phase equilibria in inclusion–host systems. *Earth and Planetary Science Letters,157*(3-4), 209-222. doi:10.1016/s0012-821x(98)00036-3

APPENDIX

Tables

Table A.1. Mineral assemblages in samples FH-1M and Z3H. X's denote presence. Margarite was not directly observed but was reported in Selverstone et al. (1984).

Sample	Hornblende	Kyanite	Staurolite	Garnet	Biotite	Chlorite	Paragonite	Plagioclase	Epidote	Ankerite	Quartz	Ilmenite	Margarite	Cummingtonite
FH-1M	x	x	x	x	x	x	x	x	x	x	x	x	(x)	
Z3H	x			x	x	x		x	x	x	x	x		x

Table A.2. Bulk compositions for FH-1M and Z3H using both XMapTools and EDS section scanning technique. * = derived from XMapTools.

Wt%	FH1M Whole Rock (XMap)	FH1M Grt-Free (XMap)	FH1M Whole Rock (EDS)	FH1M Grt-Free (EDS)	Z3H Whole Rock (XMap)	Z3H Grt-Free (XMap)	Z3H Whole Rock (EDS)	Z3H Grt-Free (EDS)
SiO2	52.09	45.59	45.86	39.35	66.29	57.95	77.28	63.94
Al2O3	20.43	16.74	22.31	18.62	15.00	10.22	12.81	8.03
TiO2	0.19	0.19	1.09	1.09	0.04	0.04	0.23	0.23
FeO	12.77	7.43	12.77*	7.43	9.04	2.45	9.03*	2.45
MgO	3.68	3.23	3.93	3.48	1.34	1.03	1.03	0.71
MnO	0.61	0.11	0.61*	0.11	0.77	0.03	0.77*	0.03
CaO	6.24	5.26	6.86	5.88	3.66	1.93	2.83	1.10
K2O	0.52	0.52	0.43	0.43	0.09	0.09	0.09	0.09
Na2O	3.47	3.47	4.97	4.97	3.76	3.76	5.86	5.86
SumOx:	100.00	82.53	98.83	81.36	100.00	77.50	104.93	81.61

Table A.3. Representative garnet compositions normalized to 12 oxygens and mole fractions of X_{Alm}, X_{Prp}, X_{Sps}, and X_{Grs} for FH-1M and Z3H samples.

	FH1M Core	FH1M Rim	Z3H Core	Z3H Rim
Si	2.97	2.98	2.97	2.97
Al	1.99	2.01	2.01	2.01
Ti	0.00	0.00	0.00	0.00
Fe^{2+}	2.05	1.92	1.96	2.24
Mg	0.31	0.55	0.17	0.33
Mn	0.19	0.22	0.22	0.09
Ca	0.48	0.33	0.66	0.33
K	0.00	0.00	0.00	0.000
Na	0.00	0.00	0.00	0.000
Total:	7.99	8.01	7.99	7.97
Wt% total	100.4	100.6	100.7	100.7
X_{Alm}	0.677	0.634	0.651	0.746

X_{Prp}	0.101	0.183	0.056	0.111
X_{Sps}	0.064	0.074	0.074	0.033
X_{Grs}	0.158	0.109	0.219	0.110
Fe/(Fe+Mg)	0.870	0.776	0.921	0.871

Table A.4. Different thermodynamic programs and their associated solution models used to create mineral assemblage diagrams.

Program	Thermo-dataset	Solution Models	Mineral Phases
Perple_X (FH1M Test1-2)	HP11	Feldspar (Fuhrman and Lindsley, 1988), Chl(White et al., 2014), Bi(White et al., 2014), Mica (White et al., 2014), cAmph(Green et al., 2016), Ctd(White et al., 2014), St(White et al., 2014), Gt(White et al., 2005), Omph(Green et al., 2007)), Ilm(White et al., 2005), Ep(Holland and Powell, 2011)	Failed to produce MAD
Perple_X (FH1M Test3)	HP11	Feldspar (Fuhrman and Lindsley, 1988), Chl(Holland et al., 1998), Bio(Holland and Powell, 1999), Mica (Smye et al., 2010), Ca-Amph(Dale et al., 2000), Ctd(Smye et al., 2010), St(White et al., 2014), Gt(White et al., 2005), Omph(Green et al., 2007), Ilm(White et al., 2014),Ep(Holland and Powell, 2011)	Gt, Bt, Ms, Om, ab, sph, ru, ilm, naph, herc, Cl, zo, ne,q

Perple_X (FH1M Test4)	HP11	Feldspar (Fuhrman and Lindsley, 1988), Chl(Holland et al., 1998), Bio(Holland and Powell, 1999), Mica (Smye et al., 2010), Amph(Dale et al., 2005), Ctd(Smye et al., 2010), St(White et al., 2014), Gt(White et al., 2005), Omph(Green et al., 2007), Ilm(White et al., 2014), Ep(Holland and Powell, 2011)	Gt, Bt, Ms, Om, ab, sph, ru, ilm, Amph, Ctd, naph, herc, Cl, ne, fa, Ep, mt,q
Perple_X(FH1M Test5)	HP11	Feldspar (Fuhrman and Lindsley, 1988), Chl(Holland et al., 1998), Bio(Holland and Powell, 1999), Mica (Smye et al., 2010), Amph(Dale et al. (2005), Ctd(Smye et al., 2010), St(White et al., 2014), Gt(White et al., 2005), Omph(Green et al., 2007), Ilm(White et al., 2014), Ep(Holland and Powell, 2011)	Gt, Bt, Ms, Om, ab, sph, ru, ilm, Amph, Ctd, naph, herc, Cl, ne, fa, Ep, mt,q (Same as test 4)

Perple_X(Z3H Test1)	HP11	Feldspar (Fuhrman and Lindsley, 1988), Chl(Holland et al., 1998), Bio(Holland and Powell, 1999), Mica (Smye et al., 2010), Amph(Dale et al., 2005), Ctd(Smye et al., 2010), St(White et al., 2014), Gt(White et al., 2005), Omph(Green et al., 2007), Ilm(White et al., 2014),Ep(Holland and Powell, 2011), oCcM(Franzolin et al., 2011)	Gt, Bt, Ms, Om, Amph, sph, gl_dqf, ab, ta, Pl, Ilm, Cl, fanth, mt,Ep, q, zo, mstp, law (core), ru (core)
Theriak Domino (FH1M)	tcbd55c2dFG/HP98	H2O, CO2, CCDO, FSP, CHTD, CRPH, CHLR, PHNG, BIO, TALC, STAU, ClAMP, CORD, SPIN, OSUM0, LIQtc, ILM, GARNET	Ilm, chlr, phng, bio, clamp, zo, H2O, arag, sph, ank, sid, q, ru, ccdo, garnet, fsp,
Theriak Domino (Z3H)	tcbd55c2dFG/HP98	H2O, CO2, FSP, ILM, GARNET, CHTD, CRPH, CHLR, PHNG, BIO, TALC, STAU, ClAMP, CORD, SPIN, OSUM0, LIQtc	Fsp, ilm, chlr, bio, clamp, q, H2O, fanth, zo, phng, sph, garnet, law, fd, LIQtc

Table A.5. Table showing the 128, 206, and 464 peak shifts for each quartz inclusion in the FH-1M garnet. Numbers correspond with inclusion numbers on figure 8.

Inclusion Number	128 Peak Shift	206 peak Shift	464 peak Shift
1	1.950	8.917	3.311
2	2.089	8.830	3.377
3	1.612	6.685	2.635
4	1.485	6.449	2.497
5	1.333	5.792	2.158
6	1.387	6.975	2.961
7	2.149	8.149	3.256
8	1.249	5.631	2.411
9	1.585	0.815	3.064
10	1.465	6.327	2.815

Table A.6. Table showing the 128, 206, and 464 peak shifts for each quartz inclusion in the Z3H garnet. Numbers correspond with inclusion numbers on figure 9.

Inclusion Number	128 Peak Shift	206 Peak Shift	464 Peak Shift
1	1.643	4.922	2.702
2	1.393	7.395	2.416
3	1.555	7.626	2.862
4	1.595	6.654	2.531
5	1.612	6.332	2.642
6	0.755	1.726	0.523
7	1.617	6.093	2.384
8	1.039	4.415	1.573
9	1.366	2.991	2.095
10	1.098	3.339	1.144
11	0.925	5.214	1.946
12	1.669	5.765	2.215
13	1.258	6.071	2.338

14	0.438	2.332	1.098
15	-0.192	1.196	0.638
16	2.037	7.818	2.854
17	0.747	3.740	1.528
18	1.850	7.233	2.592
19	0.879	3.053	1.422
20	1.219	4.099	1.579
21	1.365	6.057	2.129
22	1.426	5.922	2.012
23	1.331	5.519	2.554
24	1.154	6.328	2.328
25	0.870	2.827	0.848
26	0.984	6.109	2.079
27	1.255	6.515	1.932
28	-0.060	-0.684	0.163

29	-0.437	1.275	0.402
30	2.363	6.965	3.196
31	2.174	6.256	2.839